

Quantum-Message-Passing Receiver for Quantum-Enhanced Classical Communications

Narayanan Rengaswamy* and Henry D. Pfister†

Department of Electrical and Computer Engineering,
Duke University, Durham, North Carolina 27708, USA

Kaushik P. Seshadreesan‡ and Saikat Guha§

College of Optical Sciences, University of Arizona, Tucson, Arizona 85721, USA

(Dated: March 11, 2020)

For space-based laser communications, when the mean photon number per received optical pulse is much smaller than one, there is a large gap between communications capacity—measured in bits communicated per pulse—achievable with a receiver that detects (converts from optical to electrical domain) each modulated pulse one at a time, versus with the quantum-optimal joint-detection receiver that acts on a long codeword comprised of n modulated pulses; an effect often termed *superadditive capacity*. The action of this receiver cannot be described as the detection of each individual pulse, interspersed with classical feedforward and soft-information post-processing. In this paper, we consider the simplest scenario where a large superadditive capacity is known: a pure-loss channel with a coherent-state binary phase-shift keyed (BPSK) modulation. The two BPSK states can be mapped conceptually to two non-orthogonal states of a single qubit, described by an inner product that is a function of the mean photon number of each BPSK pulse. Using this map, we derive an explicit construction of the quantum circuit of a joint-detection receiver based on a recent idea of belief-propagation with *quantum* messages (BPQM) [J. M. Renes, New J. Phys. **19**, 072001 (2017)]. We analyze this scheme rigorously and show that it achieves the quantum limit of minimum average error probability in discriminating 8 (BPSK) codewords of a length-5 binary linear code with a tree factor graph. We quantify its performance improvement over the (Dolinar) receiver that optimally detects one pulse at a time. Our result suggests that a BPQM-receiver might attain the Holevo capacity, the quantum limit of classical communication capacity, of this BPSK-modulated pure-loss channel. This suggests a new application for a small, special-purpose, photonic quantum computer capable of so-called cat-basis universal qubit logic.

I. INTRODUCTION AND BACKGROUND

A. Message-Passing Algorithms and Belief-Propagation (BP) for Decoding Linear Codes

Message-passing algorithms are used to efficiently evaluate quantities of interest in problems defined on graphs. They work by passing messages between nodes of the graph. For example, these algorithms have been successfully used for statistical inference, optimization, constraint-satisfaction problems and the graph isomorphism problem among several other applications [1–8]. In particular, *belief-propagation (BP)* is a message-passing algorithm for efficiently marginalizing joint probability density functions in statistical inference problems. The algorithm derives its name from the fact that the messages used in BP are “local” probabilities or “beliefs” (e.g., of the value of the final quantity of interest). An application of BP relevant to this paper is the decoding of linear codes using the posterior bit-wise marginals given the outputs of a classical channel [9]. It is well-known that BP exactly performs the task of optimal bit-wise maximum-a-posteriori (bit-MAP) decoding when the factor graph of the code is a tree. However, since codes with tree factor graphs have poor minimum distance [9], BP is also applied to codes whose factor graphs have cycles, e.g. low-density parity-check (LDPC) codes. Although BP does not compute the exact marginals in this case, it is still computationally more efficient than MAP, and usually performs quite well. In fact, it has been proven that, for large blocks, BP achieves the optimal MAP performance for spatially-coupled LDPC codes over the binary erasure channel [10] and binary memoryless symmetric channels [11, 12]. From a more practical perspective, BP-based decoders are routinely deployed in modern communications and data storage.

* narayanan.rengaswamy@duke.edu

† henry.pfister@duke.edu

‡ kaushiksesh@email.arizona.edu

§ saikat@optics.arizona.edu

B. Holevo Capacity of Optical Communications

Given the success of BP decoding for classical channels, it is natural to ask if it can be generalized to the quantum setting. For example, can one decode classical codes for communications over a classical-quantum channel or, more generally, perform efficient inference on graphically-represented classical data encoded in qubits. Let us consider a coherent-state binary-phase-shift-keying (BPSK) modulation for sending classical data over a pure-loss bosonic channel of transmissivity $\eta \in (0, 1]$ [13]. The transmitter modulates each transmitted mode (i.e., “use” of the quantum channel) in one of the two states $|\alpha\rangle$ or $|- \alpha\rangle$, $\alpha \in \mathbb{R}$, with mean photon number per mode $|\alpha|^2 = N_S$. Each channel output is one of the two coherent states $|\pm \beta\rangle$, with $\beta = \sqrt{\eta}\alpha$ and mean photon number $N = \eta N_S$. These two states are non-orthogonal with an inner product $\langle \beta| - \beta\rangle = e^{-2N} \equiv \sigma$. In this case the coherent states $|\pm \beta\rangle = \sum_{n=0}^{\infty} e^{-|\beta|^2/2} \frac{(\pm \beta)^n}{\sqrt{n!}} |n\rangle$ live in an infinite-dimensional Hilbert space spanned by the complete orthonormal number basis $\{|n\rangle, n \in \mathbb{N}\}$. But, each channel output is always one of the two states $|\pm \beta\rangle$ and, for the purposes of designing a receiver, we can embed the subspace spanned by $|\pm \beta\rangle$ in a two-dimensional (qubit) Hilbert space via the inner-product-preserving map:

$$|\pm \beta\rangle \mapsto |\pm \theta\rangle := \cos \frac{\theta}{2} |0\rangle \pm \sin \frac{\theta}{2} |1\rangle, \quad (1)$$

with $\sigma = \cos \theta$. The resulting channel from a classical encoding variable x to a conditional quantum state, i.e., $[x = 0] \mapsto |\theta\rangle, [x = 1] \mapsto |-\theta\rangle$, is often called a (pure-state) *classical-quantum* (CQ) channel in the quantum information theory literature.

Let us consider a receiver that detects each channel symbol one at a time, discriminating the equally-likely $|\pm \beta\rangle$ states at the Helstrom bound [14, 15], i.e., with the minimum average probability of error $p := \frac{1}{2}[1 - \sqrt{1 - \sigma^2}]$. A structured optical design of a receiver that achieves this performance was invented by Dolinar in 1973 [16]. This receiver induces a binary symmetric channel (BSC) between the quantum channel outputs $|\pm \beta\rangle$ and the receiver’s guess “ $\pm \beta$ ”, with crossover probability p , thereby enabling the communicating parties to achieve a reliable communication rate given by $C_1 = 1 - h_2(p)$ bits per mode, the Shannon capacity of the BSC. To achieve communication at rate close to this capacity, one would need to use a code that achieves the Shannon capacity of the BSC, e.g., Arikan’s polar code [17], and a suitable decoder. If the receiver detects, i.e., converts from the quantum (optical) to the electrical domain, each quantum channel output one at a time, no amount of classical post-processing, including feedforward between channel uses, and soft-information processing, can achieve a rate higher than C_1 . For example, a BSC-capacity-achieving linear code and a BP decoder will achieve rate strictly below C_1 . It turns out however, that if the receiver is allowed to employ a quantum joint-detection receiver over a long (code) block of n channel outputs, the maximum attainable capacity is given by the Holevo limit, $C_{\infty} = S(\frac{1}{2}|\beta\rangle\langle\beta| + \frac{1}{2}|-\beta\rangle\langle-\beta|) = h_2([1 + \sigma]/2)$ bits per mode. In the limit of low received mean photon number per mode, i.e., $N \rightarrow 0$, or equivalently $\sigma \rightarrow 1$, the ratio $C_{\infty}/C_1 \rightarrow \infty$. This regime of operation is especially important for deep-space laser communications. In order to fully exploit this large capacity gain, the transmitter must use a Holevo-capacity-achieving code. For example, one could use a classical-quantum polar code [13] where the receiver acts collectively on a long modulated codeword (while still in the quantum domain). In general, consider a codebook comprising $M = 2^{nR}$ random n -mode codewords, where $R < C_{\infty}$, with each symbol of each codeword chosen from an equal prior over the two BPSK symbols. If the receiver employs the joint (Helstrom) measurement that discriminates the codewords at the minimum probability of error permissible by quantum mechanics, then the probability of decoding error goes to 0 as $n \rightarrow \infty$. This joint measurement allows the receiver to faithfully discriminate up to $2^{nC_{\infty}}$ codewords, as opposed to only 2^{nC_1} codewords if a symbol-by-symbol detection were used by the receiver. Given the quantum states of the M codewords, the optimal Helstrom measurement (projectors) can be evaluated in principle using the Yuen-Kennedy-Lax (YKL) conditions [18] applied to the Gram matrix of the codebook—the M -by- M matrix of pairwise inner products of the codewords’ quantum states. This calculation is simpler for linear codes, especially codes that have certain group symmetries [19]. Even when it is possible to compute this Helstrom measurement for the codebook, it may be hard to translate the mathematical description into a physical receiver design, unless we have a general-purpose photonic quantum computer [20]. Therefore, an efficient and physically-realizable receiver is very desirable and of significant practical interest, as long as it outperforms what is attainable with the optimal symbol-by-symbol receiver measurement.

C. Background on Belief-Propagation with Quantum Messages (BPQM)

Renes [21] recently proposed a quantum generalization of BP for a binary-output pure-state CQ channel, as discussed in Section I B. Renes’ algorithm is well-defined on a tree factor graph and works by passing quantum messages (encoded in qubits) and classical messages (bits) between nodes of the code’s factor graph. Unlike earlier algorithms termed

quantum belief-propagation [22, 23], Renes' algorithm does not measure the n channel outputs, followed by classical BP on the (classical) syndrome measurements, and hence is not limited to achieving a rate of C_1 . In order to avoid any confusion with previous “quantum belief-propagation” algorithms, we will refer to Renes' algorithm as *belief-propagation with quantum messages (BPQM)*.

In [21], the first step in developing BPQM was to interpret the message-combining operations in classical BP as “channel combining” rules that execute a local inference procedure. This step has close connections with the channel combining operation defined by Arikan for polar codes [17]. The second step was a generalization of these channel combining rules to allow for quantum messages, as in CQ polar codes [24], i.e., messages that are qubit density matrices which capture the node's belief about a message bit. The above rules define a CQ channel that gets induced at each node when (quantum) messages arrive at it. Finally, the third step was to define appropriate unitary operations at the nodes, which process the outputs of the aforesaid induced CQ channels and produce messages to be passed on to subsequent nodes.

II. MAIN RESULTS

The purpose of this paper is to provide a clear and deep study of BPQM, both its sequence of operations and its performance, and identify some of the important problems that need a detailed investigation. Despite its genesis in a logical extension of classical BP, through the generalization of the channel-combining operations at check and variable nodes, BPQM is a legitimate joint measurement (unlike its quantum BP predecessors) because it passes quantum messages, and can thereby potentially perform better than symbol-by-symbol measurements followed by optimal classical block-MAP decoding.

Even though Ref. [21] provided a phenomenological description of BPQM, there has been no performance evaluation of it for real codes and comparisons with the optimal symbol-by-symbol measurements. There has not been any proof of decoding optimality, even for CQ codes with a tree factor graph. Finally, an explicit quantum circuit for BPQM, even at the qubit level, notwithstanding its translation to an optical receiver, has not yet been prescribed. This paper addresses all of the above deficiencies.

In this paper, we construct an explicit quantum circuit for a BPQM based receiver, and prove that it can achieve the Helstrom limit of discriminating codewords of small (e.g., $n = 5$ mode) linear BPSK codes with a tree factor graph. Hence, it outperforms the best achievable performance by the optimal symbol-by-symbol receiver measurement followed by a MAP decision. How this receiver performs for larger codes, for those whose factor graphs have cycles, and whether it achieves the Holevo limit C_∞ asymptotically, remains open for future work. Leveraging optical realizations of “cat basis” quantum logic, i.e., single- and two-qubit quantum gates in the span of coherent states $|\beta\rangle$ and $|-\beta\rangle$ [25, 26], one can translate our BPQM quantum circuit into the first fully-structured optical receiver that would be able to attain the quantum limit of minimum-error discrimination of more than two coherent states.

We begin by explaining BP with the example of a 5-bit linear code, and then develop the perspective of BP in terms of channel combining operations described above, which is particularly useful to understand the quantum generalization. Then we discuss BPQM using the same example on the BPSK pure-state channel, and provide circuits for implementing BPQM. In particular, through our analysis, we introduce a coherent rotation to be performed after decoding bit 1, which is new and not part of Renes' original BPQM scheme. This might be important in generalizing BPQM to more general codes than the specific example considered here. We explicitly state the quantum-state density matrix messages that are passed, and evaluate the performance of BPQM for this example code. For decoding bit 1, we even derive an analytical expression for the BPQM success probability. The ultimate benchmark for decoding each bit is the performance of the Helstrom measurement that optimally distinguishes the density matrices corresponding to the two values of the bit (at the channel output). We show that BPQM is optimal for deciding the value of each of the 5 bits. In Fig. 1, we plot performance curves that show the “global” performance of BPQM for the 5-bit code in terms of block (codeword) error rate, rather than the individual bit error rate, for the following strategies:

- (a) collective (optimal) Helstrom measurement on all $n = 5$ channel outputs of the received codeword,
- (b) BPQM on all channel outputs of the received codeword,
- (c) symbol-by-symbol (optimal) Helstrom measurement followed by classical (optimal) block-MAP decoding, and
- (d) symbol-by-symbol (optimal) Helstrom measurement followed by classical BP decoding.

Note that, for the last two schemes, classical processing is performed essentially for the BSC with crossover probability $p = \frac{1}{2}[1 - \sqrt{1 - \sigma^2}]$, induced by measuring each channel output with the optimal single-symbol Helstrom measurement to discriminate $|\pm\theta\rangle$.

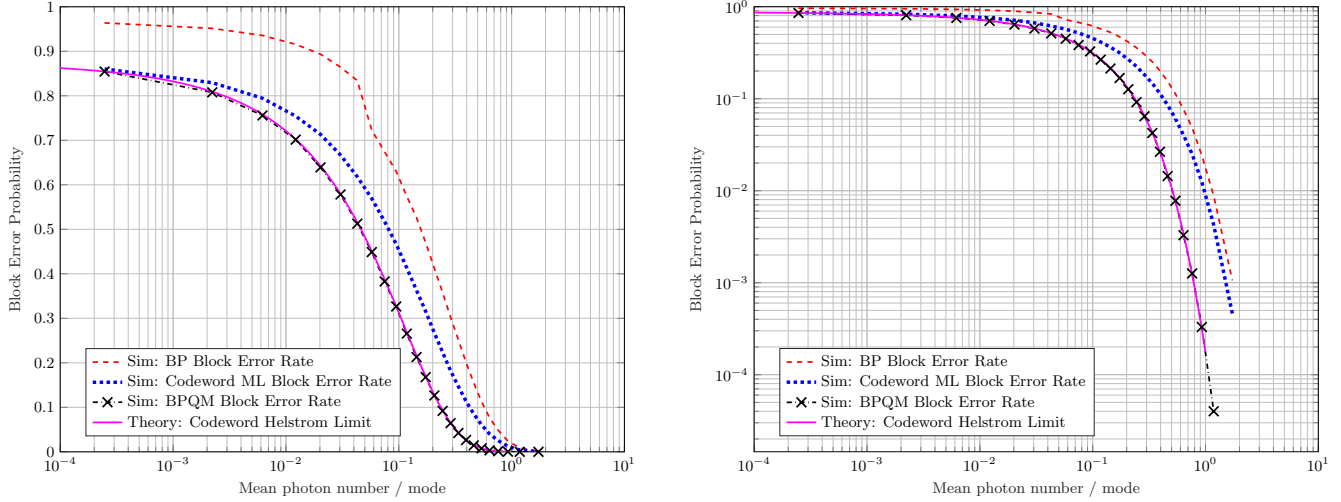


FIG. 1. The overall block error rate of BPQM along with those of quantum optimal joint Helstrom, symbol-by-symbol Helstrom followed by classical optimal block-MAP, and symbol-by-symbol Helstrom followed by classical BP.

As expected, the block error probabilities are in increasing order from (a) through (d). The plot shows that BPQM is strictly better than the quantum-optimal symbol-by-symbol detection followed by a block-MAP decision at all values of mean photon number per mode, and that it meets the optimal joint Helstrom measurement on the modulated codeword. This is an important result because, it demonstrates that, if we can construct a BPQM receiver, then it will outperform any known physically realizable receiver for this channel. We provide more detailed observations on Fig. 1 at the end of Section VD.

The paper is organized as follows. Section III discusses the classical BP algorithm and Section IV explains the BPQM algorithm. In particular, Section III A derives the BP operations by considering the problem of decoding a simple 5-bit linear code. Then Section III B develops a perspective on BP that focuses on effective channels induced during the BP node update operations. Given this background, Section IV B explains the BPQM sequence of operations in the context of the pure-state channel that is introduced in Section IV A. Subsequently, Section V discusses the decoding of the aforementioned 5-bit code over the pure-state channel, analyzes its performance, and provides the circuit for the same. In particular, Section V C carefully examines the appropriate density matrices to demonstrate the optimality of BPQM in decoding bits 2-5. Finally, Section VI concludes the paper with proposed future work.

III. CLASSICAL BELIEF-PROPAGATION (BP)

A. Decoding Linear Codes Using BP

An $[n, k, d]$ binary linear code \mathcal{C} can be defined by a binary parity-check matrix H as follows:

$$\mathcal{C} := \{\underline{x} \in \{0, 1\}^n : H\underline{x}^T = \underline{0}^T, H \in \{0, 1\}^{(n-k) \times n}\}. \quad (2)$$

Such a code encodes k message bits into n code bits, and the minimum Hamming weight of any codeword $\underline{x} \in \mathcal{C}$ is d . Consider as our running example the $[5, 3, 2]$ code, which we still denote as \mathcal{C} , defined by

$$H := \begin{bmatrix} 1 & 1 & 1 & 0 & 0 \\ 1 & 0 & 0 & 1 & 1 \end{bmatrix}. \quad (3)$$

A factor graph (FG) for a linear code is a bipartite graph where the bits (variables) are represented by circle nodes and the checks (factors) are represented by square nodes. The FG representation of (the above definition of) \mathcal{C} is shown in Fig. 2, where c_1 and c_2 represent the two parity checks on the 5 bits of each codeword in \mathcal{C} . Observe that every linear code has multiple associated parity-check matrices, each of which forms a generator matrix for its dual code. Hence, the FG representation of a code depends on the chosen parity-check matrix.

A discrete memoryless channel is represented as W and is defined by the channel transition probability matrix $W(y|x) := \mathbb{P}[Y = y | X = x]$, which represents the probability of observing $y \in \mathcal{Y}$ at the output of the channel when its

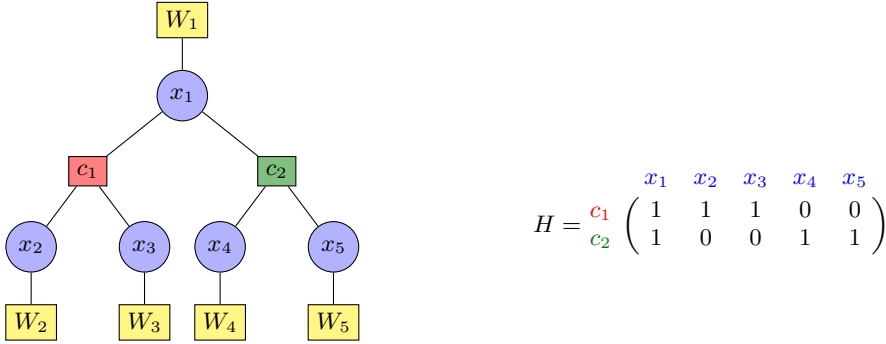


FIG. 2. Factor graph and parity-check matrix for the 5-bit linear code in the running example.

input was $x \in \mathcal{X}$. Here, \mathcal{X} and \mathcal{Y} represent the input and output alphabets of the channel, respectively. A well-known example for such a channel is the *binary symmetric channel* (BSC). For the BSC, $\mathcal{Y} = \{0, 1\} = \mathcal{X}$ and the transition matrix is defined as

$$W^{\text{BSC}} := \begin{bmatrix} 1-p & p \\ p & 1-p \end{bmatrix}, \quad (4)$$

where the (i, j) -th entry is $W^{\text{BSC}}(y = j|x = i)$ and $0 \leq p \leq 0.5$. The FG in Fig. 2 shows the channel W_k associated with each bit k as a separate factor node that provides the channel transition probability value for the observed output y_k for input $x_k = 0$ (and $x_k = 1$). These channels are not necessarily BSCs, but for simplicity we will assume that all bits go through the same channel, i.e., $W_k = W$ for all k .

Given the channel output vector, \underline{y} , the decoder tries to determine the codeword $\underline{x} \in \mathcal{C}$ that was actually sent at the input. The *block maximum-a-posteriori* (MAP) decoder calculates the posterior probability for each codeword in the code, given \underline{y} , and chooses the codeword with the maximum value. This is the optimal decoder in terms of block error rate. For the example 5-bit code \mathcal{C} , when all codewords are transmitted with equal probability, it calculates

$$p(\underline{x}|\underline{y}) = \frac{p(\underline{y}|\underline{x}) \cdot p(\underline{x})}{\sum_{\underline{x} \in \{0,1\}^5} p(\underline{y}|\underline{x}) \cdot p(\underline{x})} \quad (5)$$

$$= \frac{\prod_{k=1}^5 W(y_k|x_k) \cdot \mathbb{P}[\underline{x} \in \mathcal{C}]}{p(\underline{y})} \quad (6)$$

$$\propto \prod_{k=1}^5 W(y_k|x_k) \cdot [\mathbb{I}(x_1 \oplus x_2 \oplus x_3 = 0) \mathbb{I}(x_1 \oplus x_4 \oplus x_5 = 0)] \quad (7)$$

$$= W(y_1|x_1) \cdot [\mathbb{I}(x_1 \oplus x_2 \oplus x_3 = 0) W(y_2|x_2) W(y_3|x_3)] \cdot [\mathbb{I}(x_1 \oplus x_4 \oplus x_5 = 0) W(y_4|x_4) W(y_5|x_5)], \quad (8)$$

$$\hat{\underline{x}}^{\text{MAP}} := \underset{\underline{x} \in \{0,1\}^5}{\text{argmax}} p(\underline{x}|\underline{y}), \quad (9)$$

where the constant of proportionality in (7) is independent of \underline{x} . In general, the complexity of this scheme grows exponentially with the code dimension k because the block-MAP decoder calculates the posterior probability for each codeword in the code. A more efficient scheme is the *bit-MAP* decoder which marginalizes the above joint posterior for each bit and makes a decision bit-wise. Hence, to decode bit 1, the bit-MAP decoder computes

$$\hat{x}_1^{\text{MAP}} := \underset{x_1 \in \{0,1\}}{\text{argmax}} \sum_{x_2, x_3, x_4, x_5 \in \{0,1\}^4} p(\underline{x}|\underline{y}) \quad (10)$$

$$= \underset{x_1 \in \{0,1\}}{\text{argmax}} \left\{ W(y_1|x_1) \cdot \left[\sum_{x_2, x_3 \in \{0,1\}^2} \mathbb{I}(x_1 \oplus x_2 \oplus x_3 = 0) W(y_2|x_2) W(y_3|x_3) \right] \cdot \left[\sum_{x_4, x_5 \in \{0,1\}^2} \mathbb{I}(x_1 \oplus x_4 \oplus x_5 = 0) W(y_4|x_4) W(y_5|x_5) \right] \right\}. \quad (11)$$

Even though marginalizing a general joint probability distribution can have an exponentially scaling complexity in the number of involved variables, the idea of BP is that this can be done efficiently when the joint probability density factors into terms involving *disjoint* sets of variables. For example, on a tree FG as in the above 5-bit code, we can use the distributive property of addition over multiplication and compute the sums involved in the two square brackets *simultaneously*. Then the results can be pooled in one final step that takes their product and multiplies the result with $W(y_1|x_1)$. This is exactly BP on this FG, since the two local sums can be interpreted as “local beliefs” about the variable x_1 that are propagated to be combined with the “belief” from the channel observation y_1 .

Formally, the BP algorithm is initialized by setting the local channel factors $W_k = W(y_k|x_k)$ based on the observations y_k for both $x_k = 0$ and $x_k = 1$. Then the variables x_k simply pass on the message $(W(y_k|x_k = 0), W(y_k|x_k = 1))$ to their associated factor node(s) (FNs). In the first half-iteration of BP involving the FN update, the factors c_a calculate the “local belief” $\sum_{x_i \in \{0,1\}: i \in \partial a \setminus \{1\}} \mathbb{I}(\oplus_i x_i = x_1) \prod_i W(y_i|x_i)$ for both $x_1 = 0$ and $x_1 = 1$, where ∂a represents the indices of the set of variables attached to the factor $c_a, a \in \{1, 2\}$. In the next half-iteration of BP involving the variable node (VN) update, the VN x_1 combines all incoming local beliefs (including $W(y_1|x_1)$) by taking their product and renormalizing the result to make it the exact posterior marginal distribution for x_1 . Since this example has a tree FG, this completes BP for decoding the bit x_1 . A similar procedure can be executed for the other variables as well, and the whole scheme can be combined into a parallel BP schedule to compute marginals for all variables simultaneously. If the FG were not a tree, then we usually run BP for multiple iterations and in many cases this procedure converges to a fixed point of the BP algorithm, but we will ignore these details for brevity. Also, we note that it is common to take the BP messages to be log-likelihood ratios $\log \frac{W(y_k|x_k=0)}{W(y_k|x_k=1)}$ for implementation considerations, but this is not very important for the purposes of this paper.

B. Induced Channels in BP

We will find it very convenient to represent the operations performed by BP at each FN and VN abstractly as “local inference” over a “locally induced channel”. For convenience, consider a VN attached to exactly two FNs since a degree- d VN can always be analyzed sequentially with two FNs at a time. Then we have the following representation of the information at the VN.

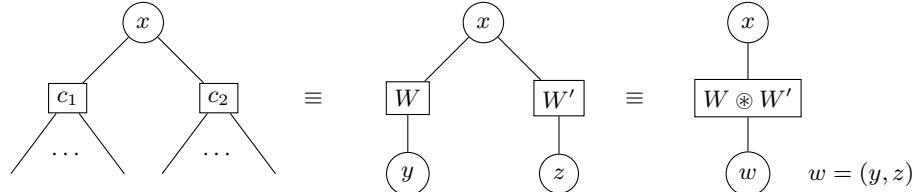


FIG. 3. Channel combining at a VN using the induced channels at the node.

In Fig. 3, all nodes other than x that are connected to c_1 and c_2 can be combined into a single value y and z , respectively, which represent *independent* observations of the variable x through some induced channels W and W' , respectively. This is because the FNs c_1 and c_2 impose a simple even parity check that ensures all attached variables sum to 0 (modulo 2). If the FNs represented a different check, then the induced channels have to be redefined accordingly. Note that the independence is exact only when the full FG is a tree. For the even parity check case, the two induced channels can be combined into a single channel $W \circledast W'$ whose outputs are the concatenation of y and z . The transition probabilities of this channel are

$$[W \circledast W'](y, z|x) = W(y|x) \cdot W'(z|x, y) \quad (12)$$

$$= W(y|x) \cdot W'(z|x). \quad (13)$$

This is called as the *variable node convolution* of two channels. Hence, during the VN update of BP, the operation is simply performing local inference over the local channel $W \circledast W'$ i.e., calculating the local posterior for x given (y, z) .

Similarly, at a (degree-3) FN we have a single input x “splitting” into two outputs u and v (since they sum to x), whose independent observations through the underlying physical channel, as well as the remaining part of the FG, are obtained as y and z . Then we have only two possibilities, either $u = x$ and $v = 0$ or $u = x \oplus 1$ and $v = 1$, and both of them are equally likely assuming that the code does not have a trivial bit position where all codewords take

the value 0. Hence, the *factor node convolution* of two channels W and W' is given by

$$[W \boxtimes W'](y, z|x) = \frac{1}{2}W(y|u=x) \cdot W'(z|v=0) + \frac{1}{2}W(y|u=x \oplus 1) \cdot W'(z|v=1) \quad (14)$$

$$= \frac{1}{2}W(y|x) \cdot W'(z|0) + \frac{1}{2}W(y|x \oplus 1) \cdot W'(z|1). \quad (15)$$

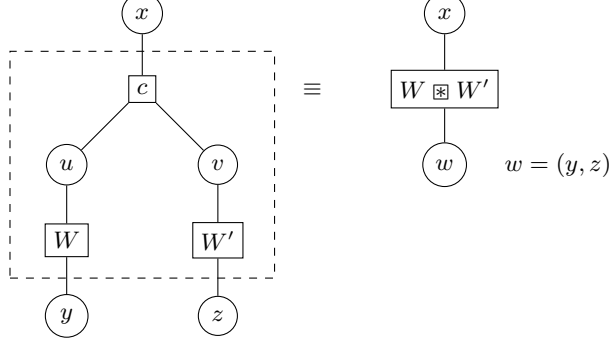


FIG. 4. Channel combining at a FN using the induced channels at the node.

We can perform a quick calculation using the FN update operation of BP to verify that BP is indeed performing local inference on this locally induced channel. In Fig. 2, consider the BP update at the FN c_1 . We observe that

$$\sum_{x_2, x_3 \in \{0, 1\}^2} \mathbb{I}(x_1 \oplus x_2 \oplus x_3 = 0) W(y_2|x_2) W(y_3|x_3) \\ = \sum_{x_2, x_3 \in \{0, 1\}^2} \mathbb{I}(x_2 \oplus x_3 = x_1) W(y_2|x_2) W(y_3|x_3) \quad (16)$$

$$= W(y_2|x_2 = x_1) \cdot W(y_3|x_3 = 0) + W(y_2|x_2 = x_1 \oplus 1) \cdot W(y_3|x_3 = 1) \quad (17)$$

$$\propto [W \boxtimes W](y_2, y_3|x_1), \quad (18)$$

where we need the factor 1/2 to make sure that it is an exact marginal (which we had omitted at the beginning of BP, in the MAP formulation, for convenience), or equivalently to ensure that $W \boxtimes W'$ is indeed a channel.

As discussed by Renes in [21], this perspective of BP crucially aids us in defining the quantum channel combining operations for a classical-quantum (CQ) channel [24] $W(x) \equiv W(|x\rangle\langle x|)$, $x \in \{0, 1\}$, as follows:

$$[W \circledast W'](x) := W(x) \otimes W'(x), \quad (19)$$

$$[W \boxtimes W'](x) := \frac{1}{2}W(x) \otimes W'(0) + \frac{1}{2}W(x \oplus 1) \otimes W'(1). \quad (20)$$

Here, we have adopted the same notation as in [21], which suppresses the outputs “ (y, z) ” that were present in the classical channel convolutions (13) and (15). This is because we do not observe the output in the quantum case unless we measure it, and measuring each channel output is not always the optimal operation at the receiver.

Remark 1. Observe that, for a general CQ channel, $W(x)$ represents the output density matrix from the channel for the classical input $x \equiv |x\rangle\langle x|$. Thus, even if the channel outputs are pure states, the induced channel at the FNs still yields a mixed state. Also note that these channels are “automatically induced by the structure of the FG”, and do not require any operation to be performed on the received states. Hence, the challenge is to identify the appropriate quantum “local inference” strategy, so that at the end of quantum BP we have performed appropriate statistical inference.

IV. BELIEF-PROPAGATION WITH QUANTUM MESSAGES (BPQM)

The idea of Renes [21] is to generalize the classical BP algorithm, which is exact for marginalization over tree FGs, to the quantum scenario where the messages can be density matrices. However, it is not immediately clear how

the posterior distribution should be defined in the quantum case because, unlike the classical case, we do not get “observations” unless we make measurements. If we indeed measure the output of each channel use, then we induce a binary-input binary-output channel whose transition probabilities depend on the measurement and the channel output density matrices $W(x)$, $x \in \{0, 1\}$. But, it is well-known that this reduces the information capacity of the channel and that collective measurements on all channel outputs may be required to achieve capacity [27]. Although this might be infeasible in practice, Renes shows that such a scheme can be simplified into a BP algorithm with quantum messages for the pure-state channel.

A. Pure-State Classical-Quantum Channel

The *pure-state channel* is defined for classical inputs $x \equiv |x\rangle\langle x|$, $x \in \{0, 1\}$, as

$$W(x) := |\theta\rangle\langle 0| \cdot |x\rangle\langle x| \cdot |\theta\rangle\langle \theta| + |-\theta\rangle\langle 1| \cdot |x\rangle\langle x| \cdot |-\theta\rangle\langle -\theta| \quad (21)$$

$$= \langle x|0\rangle \cdot |\theta\rangle\langle \theta| + \langle x|1\rangle \cdot |-\theta\rangle\langle -\theta|, \quad (22)$$

$$|\pm\theta\rangle := \cos \frac{\theta}{2} |0\rangle \pm \sin \frac{\theta}{2} |1\rangle. \quad (23)$$

Hence, the Kraus operators for the channel can be taken to be $M_0 = |\theta\rangle\langle 0|$, $M_1 = |-\theta\rangle\langle 1|$. If the input system to W is denoted by X and the output system by B , then the joint density matrix ρ_{XB} that is required to characterize the entropic quantities for this channel is given by

$$\rho_{XB} := q \cdot |0\rangle\langle 0|_X \otimes |\theta\rangle\langle \theta|_B + (1 - q) \cdot |1\rangle\langle 1|_X \otimes |-\theta\rangle\langle -\theta|_B, \quad (24)$$

where q is the prior probability for input $x = 0$. The joint (von Neumann) entropy for XB is given by

$$S(XB)_\rho = S(X) + \sum_{x \in \{0, 1\}} p_X(x) S(\rho_B^{(x)}) \quad (25)$$

$$= h_2(q) + q \cdot S(|\theta\rangle\langle \theta|_B) + (1 - q)S(|-\theta\rangle\langle -\theta|_B) \quad (26)$$

$$= h_2(q), \quad (27)$$

where $h_2(q) := -q \log_2(q) - (1 - q) \log_2(1 - q)$ (bits) is the binary entropy function and $S(|\theta\rangle\langle \theta|_B) = S(|-\theta\rangle\langle -\theta|_B) = 0$ since the states are pure. Therefore, the quantum mutual information for the pure-state channel is the symmetric Holevo information

$$I(X; B)_\rho := S(X)_\rho + S(B)_\rho - S(XB)_\rho \quad (28)$$

$$= h_2(q) + S(\rho_B) - h_2(q) \quad (29)$$

$$= S(q \cdot |\theta\rangle\langle \theta|_B + (1 - q) \cdot |-\theta\rangle\langle -\theta|_B). \quad (30)$$

The ultimate capacity for this channel in the asymptotic limit of a large number of channel uses (per use of the channel) is $\max_{q \in [0, 1]} I(X; B)_\rho = \max_{q \in [0, 1]} S(\rho_B)$. Since this channel is equivalent to the BPSK (binary phase shift keying) modulated pure-loss optical channel [13], it is known that the maximum occurs at $q = 1/2$ and hence the Holevo capacity is given by

$$C_\infty(W) = S\left(\frac{1}{2} \cdot |\theta\rangle\langle \theta|_B + \frac{1}{2} \cdot |-\theta\rangle\langle -\theta|_B\right) = h_2\left(\cos^2 \frac{\theta}{2}\right) = h_2\left(\frac{1 + \sqrt{F(W)}}{2}\right), \quad (31)$$

where the *fidelity* of the channel is $F(W) := |\langle \theta| - \theta \rangle|^2 = \cos^2 \theta$, $\cos \theta = 2 \cos^2 \frac{\theta}{2} - 1$, and the subscript “ ∞ ” indicates that one might need collective (or joint) measurements on all channel outputs to achieve capacity [13].

If, instead, we performed the Helstrom measurement at the output of each use of the channel, i.e., for each code bit sent through W , then this would induce a BSC(P_{\min}) with $P_{\min} = (1 - \sqrt{1 - F(W)})/2$, which is the minimum probability of error to distinguish between the states $\{|\theta\rangle, |-\theta\rangle\}$. The Helstrom measurement [14, 15] to optimally distinguish between two density matrices ρ_0 and ρ_1 is defined by $\{\Pi_{\text{Hel}}, \mathbb{I} - \Pi_{\text{Hel}}\}$:

$$\Pi_{\text{Hel}} := \sum_{i: \lambda_i \geq 0} |i\rangle\langle i|, \quad (\rho_0 - \rho_1)|i\rangle = \lambda_i|i\rangle. \quad (32)$$

For the pure state channel, it is easy to calculate that $\rho_0 - \rho_1 = |\theta\rangle\langle \theta| - |-\theta\rangle\langle -\theta| = \sin \theta \cdot X$ so that the Helstrom measurement is projecting onto the Pauli X basis, i.e., the POVM is $\{|+\rangle\langle +|, |-\rangle\langle -|\}$. In practice, the *Dolinar*

receiver for the BPSK modulated pure-loss optical channel induces this BSC(P_{\min}) [13]. If we implemented a classical optimal (block-MAP) decoder on this induced BSC, then the capacity that is attainable is $C_1(W) = 1 - h_2(P_{\min})$, where the subscript “1” indicates that we are performing symbol-by-symbol measurements and not a collective measurement. It can be easily checked that $C_1(W) \ll C_{\infty}(W)$, and classical-quantum polar codes equipped with a quantum successive-cancellation decoder close this gap [13, 27]. However, the optimal decoder for CQ polar codes is hard to realize in the lab. Hence, an interesting open problem is to analyze how much of this gap is closed by BPQM because it can be mapped into a “successive-cancellation-type” decoder as discussed in [21]. In fact, we will see that BPQM has a successive-cancellation flavor by definition.

B. Node Operations in BPQM

For the pure-state channel, the following operations are defined to be performed at variable nodes and factor nodes [21] (see Appendix B for detailed calculations). At a VN, the convolution $W \circledast W'$ *ideally* yields either $|\theta\rangle \otimes |\theta'\rangle$ or $|- \theta\rangle \otimes |- \theta'\rangle$. Note that the local convolution is performed with respect to input $x = 0$ and $x = 1$ separately, respectively inducing signs $+$ and $-$. We say “ideally” because we expect the signs of all incoming qubits at a VN to be the same, which means all independent local beliefs of the VN agree on the bit’s value. Since the pure-state channel does not introduce noise, and the only uncertainty arises from the non-orthogonality of $|\theta\rangle$ and $|- \theta\rangle$, the qubits always combine in this ideal fashion until the first bit is decoded. But, whether this situation continues for the next bit depends upon whether the first bit was decoded to be a 0 or 1. This is because, as mentioned earlier, the FN channel convolution in (20) is defined assuming that the FN imposes an even parity-check. If, instead, it imposed an odd parity-check, as will happen when one of the bits is decoded to be a 1, then the FN convolution has to be modified appropriately. Therefore, if the FN originally had degree 3 and one of the bits have been estimated to be 1, then we can remove the bit and update the FN to be an odd parity-check on two bits. This degree 2 FN effectively induces a modified VN convolution with the signs of the two qubits in disagreement.

Given the (ideal) convolution outputs, the following unitary is applied to “compress” the information into one qubit and force the other system to be in state $|0\rangle$:

$$U_{\circledast}(\theta, \theta') := \begin{bmatrix} a_+ & 0 & 0 & a_- \\ a_- & 0 & 0 & -a_+ \\ 0 & b_+ & b_- & 0 \\ 0 & b_- & -b_+ & 0 \end{bmatrix}, \quad (33)$$

$$a_{\pm} := \frac{1}{\sqrt{2}} \frac{\cos\left(\frac{\theta-\theta'}{2}\right) \pm \cos\left(\frac{\theta+\theta'}{2}\right)}{\sqrt{1 + \cos\theta \cos\theta'}}, \quad b_{\pm} := \frac{1}{\sqrt{2}} \frac{\sin\left(\frac{\theta+\theta'}{2}\right) \mp \sin\left(\frac{\theta-\theta'}{2}\right)}{\sqrt{1 - \cos\theta \cos\theta'}}. \quad (34)$$

Hence, we have $U_{\circledast}(\theta, \theta') (|\pm\theta\rangle \otimes |\pm\theta'\rangle) = |\pm\theta^*\rangle \otimes |0\rangle$, where $\cos\theta^* := \cos\theta \cos\theta'$. The VN update is then to just pass on the qubit in the first system and discard the second system.

At the FN, the induced mixed state $[W \boxtimes W'](x)$ can be transformed into the CQ state $\sum_{j \in \{0,1\}} p_j |\pm\theta_j^{\boxtimes}\rangle \langle \pm\theta_j^{\boxtimes}| \otimes |j\rangle \langle j|$ by performing $U_{\boxtimes} := \text{CNOT}_{W \rightarrow W'}$, the controlled-NOT gate with W as control and W' as target. Hence,

$$U_{\boxtimes} ([W \boxtimes W'](x)) U_{\boxtimes}^{\dagger} = \sum_{j \in \{0,1\}} p_j |\pm\theta_j^{\boxtimes}\rangle \langle \pm\theta_j^{\boxtimes}| \otimes |j\rangle \langle j|, \quad (35)$$

$$p_0 := \frac{1}{2}(1 + \cos\theta \cos\theta'), \quad p_1 := 1 - p_0, \quad \cos\theta_0^{\boxtimes} := \frac{\cos\theta + \cos\theta'}{1 + \cos\theta \cos\theta'}, \quad \cos\theta_1^{\boxtimes} := \frac{\cos\theta - \cos\theta'}{1 - \cos\theta \cos\theta'}. \quad (36)$$

Observe that for $j = 0$, the angle between the states has decreased, while for $j = 1$ the angle has increased. The FN update is then to measure the second system and pass the resulting qubit in the first system as the message, along with the result of the classical measurement. This is because the VN update at the next stage needs to know the angle θ, θ' of the incoming qubits. When we have a degree d node, these channel convolutions can be performed two at a time. Equivalently, we can write down a circuit composed of CNOT operations and Z -basis measurements, and use the “principle of deferred measurements” [28, Section 4.4] to delay the measurements until the end of the circuit. For clarity, we will describe BPQM as a coherent operation that does not measure or discard qubits along the way.

Remark 2. Note that in each half-iteration of BP, all VN or FN updates can be performed simultaneously since this involves only classical arithmetic and we can implicitly clone the values. This is indeed a different update schedule when compared to slower sequential updates, but can always be implemented if desired. However, in BPQM, we are forced to perform operations sequentially until one bit is decoded and then attempt to reverse the executed operations in a suitable manner. Our subsequent analysis of BPQM will assume this sequential schedule.

V. BPQM ON THE 5-BIT CODE

A. Decoding Bit 1

Let us begin by describing the procedure to decode bit 1 of the 5-bit code in our running example. Observe that the codewords belonging to the code are

$$\mathcal{C} = \{00000, 00011, 01100, 01111, 10101, 10110, 11001, 11010\}. \quad (37)$$

We assume that all the codewords are equally likely to be transmitted, just as in classical BP. Then the task of decoding the value of the first bit x_1 involves distinguishing between the density matrices $\rho_1^{(0)}$ and $\rho_1^{(1)}$, which are uniform mixtures of the states corresponding to the codewords that have $x_1 = 0$ and $x_1 = 1$, respectively, i.e.,

$$\begin{aligned} \rho_1^{(0)} = & |\theta\rangle\langle\theta|_1 \otimes \frac{1}{4} \left[|\theta\rangle\langle\theta|_2 \otimes |\theta\rangle\langle\theta|_3 \otimes |\theta\rangle\langle\theta|_4 \otimes |\theta\rangle\langle\theta|_5 + |\theta\rangle\langle\theta|_2 \otimes |\theta\rangle\langle\theta|_3 \otimes |-\theta\rangle\langle-\theta|_4 \otimes |-\theta\rangle\langle-\theta|_5 \right. \\ & \left. + |-\theta\rangle\langle-\theta|_2 \otimes |-\theta\rangle\langle-\theta|_3 \otimes |\theta\rangle\langle\theta|_4 \otimes |\theta\rangle\langle\theta|_5 + |-\theta\rangle\langle-\theta|_2 \otimes |-\theta\rangle\langle-\theta|_3 \otimes |-\theta\rangle\langle-\theta|_4 \otimes |-\theta\rangle\langle-\theta|_5 \right], \end{aligned} \quad (38)$$

$$\begin{aligned} \rho_1^{(1)} = & |-\theta\rangle\langle-\theta|_1 \otimes \frac{1}{4} \left[|\theta\rangle\langle\theta|_2 \otimes |-\theta\rangle\langle-\theta|_3 \otimes |\theta\rangle\langle\theta|_4 \otimes |-\theta\rangle\langle-\theta|_5 + |\theta\rangle\langle\theta|_2 \otimes |-\theta\rangle\langle-\theta|_3 \otimes |-\theta\rangle\langle-\theta|_4 \otimes |\theta\rangle\langle\theta|_5 \right. \\ & \left. + |-\theta\rangle\langle-\theta|_2 \otimes |\theta\rangle\langle\theta|_3 \otimes |\theta\rangle\langle\theta|_4 \otimes |-\theta\rangle\langle-\theta|_5 + |-\theta\rangle\langle-\theta|_2 \otimes |\theta\rangle\langle\theta|_3 \otimes |-\theta\rangle\langle-\theta|_4 \otimes |\theta\rangle\langle\theta|_5 \right]. \end{aligned} \quad (39)$$

These density matrices can be written in terms of the FN channel convolution in (20) as $\rho_1^{x_1} = \rho_{\pm} = |\pm\theta\rangle\langle\pm\theta|_1 \otimes [W \boxtimes W](x_1)_{23} \otimes [W \boxtimes W](x_1)_{45}$, where we use the notation $\pm \equiv (-1)^{x_1}$, $x_1 \in \{0, 1\}$.

The BPQM circuit for decoding x_1 is shown in Fig. 5 along with the density matrix in each stage of the circuit denoted by (a) through (e).

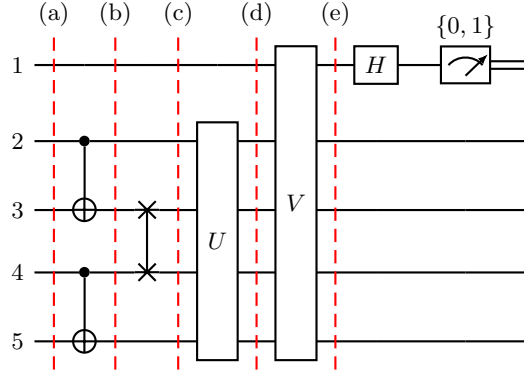


FIG. 5. The BPQM circuit to decode bit 1 of the 5-bit code in Fig. 2. All circuits are drawn using the ‘‘Quantikz’’ package [29].

- (a) $\rho_{\pm,a} = |\pm\theta\rangle\langle\pm\theta|_1 \otimes [W \boxtimes W](x_1)_{23} \otimes [W \boxtimes W](x_1)_{45}$.
- (b) $\rho_{\pm,b} = |\pm\theta\rangle\langle\pm\theta|_1 \otimes \sum_{j \in \{0,1\}} p_j |\pm\theta_j^{\boxtimes}\rangle\langle\pm\theta_j^{\boxtimes}|_2 \otimes |j\rangle\langle j|_3 \otimes \sum_{k \in \{0,1\}} p_k |\pm\theta_k^{\boxtimes}\rangle\langle\pm\theta_k^{\boxtimes}|_4 \otimes |k\rangle\langle k|_5$.
- (c) $\rho_{\pm,c} = |\pm\theta\rangle\langle\pm\theta|_1 \otimes \sum_{j,k \in \{0,1\}^2} p_j p_k |\pm\theta_j^{\boxtimes}\rangle\langle\pm\theta_j^{\boxtimes}|_2 \otimes |\pm\theta_k^{\boxtimes}\rangle\langle\pm\theta_k^{\boxtimes}|_3 \otimes |j\rangle\langle j|_4 \otimes |k\rangle\langle k|_5$.
- (d) $\sigma_{\pm} = \sum_{j,k \in \{0,1\}^2} p_j p_k |\pm\theta\rangle\langle\pm\theta|_1 \otimes |\pm\theta_{jk}^{\boxtimes}\rangle\langle\pm\theta_{jk}^{\boxtimes}|_2 \otimes |0\rangle\langle 0|_3 \otimes |jk\rangle\langle jk|_{45}$, where the applied unitary operation is $U := \sum_{j,k \in \{0,1\}^2} U_{\boxtimes}(\theta_j^{\boxtimes}, \theta_k^{\boxtimes})_{23} \otimes |jk\rangle\langle jk|_{45}$ and $\cos\theta_{jk}^{\boxtimes} := \cos\theta_j^{\boxtimes} \cos\theta_k^{\boxtimes}$.
- (e) $\Psi_{\pm} = \sum_{j,k \in \{0,1\}^2} p_j p_k |\pm\varphi_{jk}^{\boxtimes}\rangle\langle\pm\varphi_{jk}^{\boxtimes}|_1 \otimes |0\rangle\langle 0|_2 \otimes |0\rangle\langle 0|_3 \otimes |jk\rangle\langle jk|_{45}$, where the applied unitary operation is $V := \sum_{j,k \in \{0,1\}^2} U_{\boxtimes}(\theta, \theta_{jk}^{\boxtimes})_{12} \otimes |jk\rangle\langle jk|_{45}$ and $\cos\varphi_{jk}^{\boxtimes} := \cos\theta \cos\theta_{jk}^{\boxtimes}$.

We emphasize that at each stage, the density matrix is the *expectation* over all pure states obtained there that correspond to transmitted codewords with the first bit taking value $x_1 \in \{0, 1\}$. The operations U and V are effectively two-qubit unitary operations, albeit controlled ones, and this phenomenon extends to any factor graph. Evidently, BPQM compresses all the quantum information into system 1 and the problem reduces to distinguishing between $\Psi_{\pm}^{(1)} = \sum_{j,k \in \{0,1\}^2} p_j p_k \left| \pm \varphi_{jk}^{\circledast} \right\rangle \left\langle \pm \varphi_{jk}^{\circledast} \right|_1$, since the other systems are either trivial or completely classical and independent of x_1 . Finally, system 1 is measured by projecting onto the Pauli X basis, which we know from the discussion in Section IV A after (32) to be the Helstrom measurement to optimally distinguish between the states $\Psi_{\pm}^{(1)}$.

It is pertinent that the optimal success probability of distinguishing between the density matrices $\rho_1^{(0)}$ and $\rho_1^{(1)}$ using a collective Helstrom measurement is given by

$$P_{\text{succ},1}^{\text{Hel}} = \frac{1}{2} + \frac{1}{4} \left\| \rho_1^{(0)} - \rho_1^{(1)} \right\|_1, \quad \|M\|_1 := \text{Tr} \left(\sqrt{M^{\dagger} M} \right). \quad (40)$$

The action of BPQM until the final measurement is unitary and the trace norm $\|\cdot\|_1$ is invariant under unitaries. Thus, BPQM does not lose optimality until the final measurement. Since the final measurement is also optimal for distinguishing the two possible states at that stage (e), BPQM is indeed optimal in decoding the value of x_1 . Thus, despite not performing a collective measurement, but rather only a *single-qubit measurement* at the end of a sequence of unitaries motivated by the FG structure and induced channels in classical BP, BPQM is still optimal to determine whether $x_1 = 0$ or 1. The performance curves plotted in Fig. 6 demonstrate this optimality.

Remark 3. *Observe that in this quantum scenario, $\rho_1^{(x)}$ behave like a “posterior” for bit x_1 . However, these can be written down even before transmitting over the channel since they do not depend on the output of the channel. Hence, it is unclear if there is a better notion of a true posterior which we can then show to be “marginalized” by BPQM.*

Performance Analysis

For bit x_1 , the probability to decode it as $\hat{x}_1 = 0$ is

$$\mathbb{P} \left[\hat{x}_1 = 0 \mid \Psi_{\pm}^{(1)} \right] = \text{Tr} \left[\Psi_{\pm}^{(1)} \left| + \right\rangle \left\langle + \right| \right] = \sum_{j,k \in \{0,1\}^2} p_j p_k \left(\frac{1 \pm \sin \varphi_{jk}^{\circledast}}{2} \right). \quad (41)$$

Therefore, since there are 4 codewords each that have $x_1 = 0$ and $x_1 = 1$, the prior for bit x_1 is 1/2 and the probability of success for BPQM in decoding the bit x_1 is

$$P_{\text{succ},1}^{\text{BPQM}} = \mathbb{P}[x_1 = 0] \cdot \mathbb{P}[\hat{x}_1 = 0 \mid x_1 = 0] + \mathbb{P}[x_1 = 1] \cdot \mathbb{P}[\hat{x}_1 = 1 \mid x_1 = 1] \quad (42)$$

$$= \frac{1}{2} \left[\sum_{j,k \in \{0,1\}^2} p_j p_k \left(\frac{1 + \sin \varphi_{jk}^{\circledast}}{2} \right) + \sum_{j,k \in \{0,1\}^2} p_j p_k \left(\frac{1 - \sin \varphi_{jk}^{\circledast}}{2} \right) \right] \quad (43)$$

$$= \frac{p_0^2}{2} (1 + \sin \varphi_{00}^{\circledast}) + (1 - p_0^2) \quad (44)$$

$$= 1 - \frac{p_0^2}{2} (1 - \sin \varphi_{00}^{\circledast}), \quad (45)$$

where we have used the fact that since all channels are identically W , we have $\cos \theta_1^{\boxtimes} = 0$. We can calculate

$$\cos \varphi_{00}^{\circledast} = \cos \theta \cos \theta_{00}^{\circledast} = \cos \theta \cos^2 \theta_0^{\boxtimes} = \cos \theta \frac{4 \cos^2 \theta}{(1 + \cos^2 \theta)^2} \quad (46)$$

$$\Rightarrow \sin \varphi_{00}^{\circledast} = \sqrt{1 - \frac{16 \cos^6 \theta}{(1 + \cos^2 \theta)^4}} = \sqrt{1 - \frac{(2p_0 - 1)^3}{p_0^4}} = \frac{\sqrt{p_0^4 - (2p_0 - 1)^3}}{p_0^2}. \quad (47)$$

Substituting back, we get the BPQM probability of success for bit x_1 to be

$$P_{\text{succ},1}^{\text{BPQM}} = 1 - \frac{p_0^2 - \sqrt{p_0^4 - (2p_0 - 1)^3}}{2} = P_{\text{succ},1}^{\text{Hel}}, \quad (48)$$

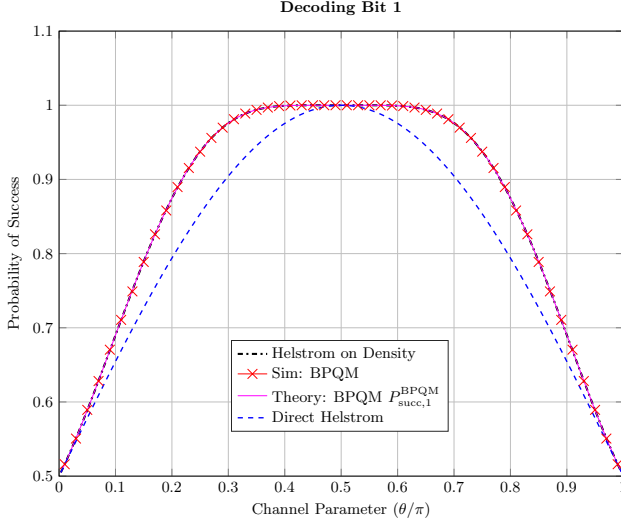


FIG. 6. The success probabilities for decoding the value of x_1 in the 5-bit code. Here, ‘‘Helstrom on Density’’ represents $P_{\text{succ},1}^{\text{Hel}}$ and ‘‘Direct’’ represents the success probability when directly implementing the Helstrom measurement at the channel output on system 1. The curve ‘‘Sim: BPQM’’ corresponds to a simulation that averaged each data point over 10^5 codewords.

which is the curve plotted as ‘‘Theory: BPQM $P_{\text{succ},1}^{\text{BPQM}}$ ’’ in Fig. 6.

Before measuring system 1, the state of system 1 is essentially $\Psi_{\pm}^{(1)} = p_0^2 |\pm\varphi_{00}^{\circledast}\rangle\langle\pm\varphi_{00}^{\circledast}| + (1 - p_0^2) |\pm\rangle\langle\pm|$, since $\cos\varphi_{jk}^{\circledast} = 0$ whenever either j or k equals 1 (or both) and hence $|\pm\varphi_{jk}^{\circledast}\rangle\langle\pm\varphi_{jk}^{\circledast}| = |\pm\rangle\langle\pm|$. So, p_0^2 is the probability that the system ‘‘confuses’’ the decoder, and projection onto the X basis essentially replaces the system with $|m_1\rangle\langle m_1|$, where $m_1 = (-1)^{\hat{x}_1} \in \{+, -\}$. The full post-measurement state is given by quantum mechanics to be

$$\Phi_{m_1} = \sum_{j,k \in \{0,1\}^2} p_j p_k \frac{|\langle m_1 | \pm\varphi_{jk}^{\circledast} \rangle|^2}{\text{Tr} [\Psi_{\pm}^{(1)} |m_1\rangle\langle m_1|]} |m_1\rangle\langle m_1|_1 \otimes |00\rangle\langle 00|_{23} \otimes |jk\rangle\langle jk|_{45}. \quad (49)$$

Note that in Fig. 5, we need to apply a Hadamard after the Z -basis measurement in order to ensure that the effective projector is $H|\hat{x}_1\rangle\langle\hat{x}_1|H = |m_1\rangle\langle m_1|$.

Let us denote the overall unitary operation performed in Fig. 5 until stage (e) as B_1^{BPQM} . As mentioned earlier, the Helstrom measurement to optimally distinguish between $\rho_1^{(0)}$ and $\rho_1^{(1)}$ is given by the POVM $\{\Pi_1^{\text{Hel}}, \mathbb{I} - \Pi_1^{\text{Hel}}\}$, where

$$\Pi_1^{\text{Hel}} := \sum_{i: \lambda_i \geq 0} |i\rangle\langle i|, \quad (\rho_1^{(0)} - \rho_1^{(1)}) |i\rangle = \lambda_i |i\rangle. \quad (50)$$

BPQM performs the final Helstrom measurement given by the POVM $\{\tilde{\Pi}_1^{\text{Hel}}, \mathbb{I} - \tilde{\Pi}_1^{\text{Hel}}\}$, where

$$\tilde{\Pi}_1^{\text{Hel}} := \sum_{j: \lambda_j \geq 0} |j\rangle\langle j| = |+\rangle\langle +|_1 \otimes (I_{16})_{2345}, \quad (\Psi_+ - \Psi_-) |j\rangle = \lambda_j |j\rangle \quad (51)$$

$$\Rightarrow \left[B_1^{\text{BPQM}} \rho_1^{(0)} \left(B_1^{\text{BPQM}} \right)^{\dagger} - B_1^{\text{BPQM}} \rho_1^{(1)} \left(B_1^{\text{BPQM}} \right)^{\dagger} \right] |j\rangle = \lambda_j |j\rangle \quad (52)$$

$$\Rightarrow (\rho_1^{(0)} - \rho_1^{(1)}) \left(B_1^{\text{BPQM}} \right)^{\dagger} |j\rangle = \lambda_j \left(B_1^{\text{BPQM}} \right)^{\dagger} |j\rangle. \quad (53)$$

Thus, we can express the eigenvectors for $(\rho_1^{(0)} - \rho_1^{(1)})$ as $|i\rangle = \left(B_1^{\text{BPQM}} \right)^{\dagger} |j\rangle$. This further implies that

$$\Pi_1^{\text{Hel}} = \sum_{i: \lambda_i \geq 0} |i\rangle\langle i| = \left(B_1^{\text{BPQM}} \right)^{\dagger} \left[\sum_{j: \lambda_j \geq 0} |j\rangle\langle j| \right] B_1^{\text{BPQM}} = \left(B_1^{\text{BPQM}} \right)^{\dagger} [|+\rangle\langle +|_1 \otimes (I_{16})_{2345}] B_1^{\text{BPQM}}. \quad (54)$$

Hence, in order to identically apply the Helstrom measurement Π_1^{Hel} , BPQM needs to first apply B_1^{BPQM} , then measure the first qubit in the X -basis, and finally invert B_1^{BPQM} on the post-measurement state Φ_{m_1} above. Although this is optimal for bit 1, next we will see that it is beneficial to coherently rotate Φ_{m_1} before inverting B_1^{BPQM} , which sets up a better state discrimination problem for decoding bit 2.

B. Decoding Bits 2 and 3 (or 4 and 5)

Next, in order to execute BPQM to decode bit x_2 , we would ideally hope to change the state Φ_{m_1} back to the channel outputs. However, this is impossible after having performed the measurement. In the original BPQM algorithm [21], the procedure to be performed at this stage is ambiguous, so we describe a strategy that treads closely along the path of performing the Helstrom measurement for bit 2 as well, i.e., optimally distinguishing $\rho_2^{(0)}$ and $\rho_2^{(1)}$ evolved through $\tilde{A}_1^{\text{BPQM}} := (B_1^{\text{BPQM}})^\dagger [m_1] \langle m_1|_1 \otimes (I_{16})_{2345}] B_1^{\text{BPQM}}$.

In order to be able to run BPQM for bit x_1 in reverse to get “as close” to the channel outputs as possible, we need to make sure that the state Φ_{m_1} is modified to be compatible with the (angles used to define the) unitaries V and U in Fig. 5. Since we can keep track of the intermediate angles deterministically, we can conditionally rotate subsystem 1 to be $|m_1\varphi_{00}^*\rangle \langle m_1\varphi_{00}^*|_1$ for $|jk\rangle \langle jk|_{45} = |00\rangle \langle 00|_{45}$. Note again that in Ψ_\pm , when either of j or k is 1 (or both), $\varphi_{jk}^* = \pi/2$ and hence $|\pm\varphi_{jk}^*\rangle \langle \pm\varphi_{jk}^*| = |\pm\rangle \langle \pm|$. Therefore, if \hat{x}_1 is the wrong estimate for x_1 , then $\langle m_1|\pm\rangle = 0$ and the superposition in Φ_{m_1} collapses to a single term with $j = k = 0$.

More precisely, we can implement the unitary operation (see Appendix A for a decomposition of K_{m_1})

$$M_{m_1} := (K_{m_1})_1 \otimes |00\rangle \langle 00|_{45} + (I_2)_1 \otimes (|01\rangle \langle 01|_{45} + |10\rangle \langle 10|_{45} + |11\rangle \langle 11|_{45}), \quad (55)$$

where K_+ and K_- are unitaries chosen to satisfy $K_+|+\rangle = |\varphi_{00}^*\rangle$ and $K_-|-\rangle = |-\varphi_{00}^*\rangle$, respectively. We can easily complete these partially defined unitaries with the conditions $K_+|-\rangle = \sin \frac{\varphi_{00}^*}{2} |0\rangle - \cos \frac{\varphi_{00}^*}{2} |1\rangle$ and $K_-|+\rangle = \sin \frac{\varphi_{00}^*}{2} |0\rangle + \cos \frac{\varphi_{00}^*}{2} |1\rangle$. Applying M_{m_1} to Φ_{m_1} we get the desired state (compare to state Ψ_\pm in stage (e) of Fig. 5)

$$\tilde{\Psi}_{m_1} = \sum_{j,k \in \{0,1\}^2} p_j p_k \frac{\left| \langle m_1 | \pm \varphi_{jk}^* \rangle \right|^2}{\text{Tr} [\Psi_\pm^{(1)} |m_1\rangle \langle m_1|]} |m_1\varphi_{jk}^*\rangle \langle m_1\varphi_{jk}^*|_1 \otimes |00\rangle \langle 00|_{23} \otimes |jk\rangle \langle jk|_{45}. \quad (56)$$

Now the BPQM circuit for bit x_1 , shown in Fig. 5, can be run in reverse from before the final measurement, i.e., from stage (e) back to stage (a). Hence, the overall operation on the input state in Fig. 5 is

$$A_1^{\text{BPQM}} := (B_1^{\text{BPQM}})^\dagger M_{m_1} [m_1] \langle m_1|_1 \otimes (I_{16})_{2345}] B_1^{\text{BPQM}}. \quad (57)$$

Then we expect the state to be almost the same as the channel outputs, except that system 1 will deterministically be in state $|m_1\theta\rangle \langle m_1\theta|_1$. However, a simple calculation shows that this is not completely true since the additional factor $\frac{|\langle m_1 | \pm \varphi_{jk}^* \rangle|^2}{\text{Tr} [\Psi_\pm^{(1)} |m_1\rangle \langle m_1|]}$ prevents the density matrix to decompose into a tensor product of two 2-qubit density matrices at stage (b) of Fig. 5. Specifically, when we take $\tilde{\Psi}_{m_1}$ at stage (e) back to stage (b) by inverting the BPQM operations, we arrive at the state

$$\tilde{\rho}_{\pm,b}^{(m_1)} = |m_1\theta\rangle \langle m_1\theta|_1 \otimes \sum_{j,k \in \{0,1\}^2} p_j p_k \frac{\left| \langle m_1 | \pm \varphi_{jk}^* \rangle \right|^2}{\text{Tr} [\Psi_\pm^{(1)} |m_1\rangle \langle m_1|]} \left(|m_1\theta_j^{\boxtimes}\rangle \langle m_1\theta_j^{\boxtimes}|_2 \otimes |j\rangle \langle j|_3 \right) \otimes \left(|m_1\theta_k^{\boxtimes}\rangle \langle m_1\theta_k^{\boxtimes}|_4 \otimes |k\rangle \langle k|_5 \right) \quad (58)$$

$$= \begin{cases} \frac{1}{P_{\text{succ},1}^{\text{BPQM}}} |m_1\theta\rangle \langle m_1\theta|_1 \otimes \sum_{j,k \in \{0,1\}^2} p_j p_k \left| \langle m_1 | \pm \varphi_{jk}^* \rangle \right|^2 \left(|m_1\theta_j^{\boxtimes}\rangle \langle m_1\theta_j^{\boxtimes}|_2 \otimes |j\rangle \langle j|_3 \right) \\ \quad \otimes \left(|m_1\theta_k^{\boxtimes}\rangle \langle m_1\theta_k^{\boxtimes}|_4 \otimes |k\rangle \langle k|_5 \right) & \text{if } \hat{x}_1 = x_1, \\ |m_1\theta\rangle \langle m_1\theta|_1 \otimes \left(|m_1\theta_0^{\boxtimes}\rangle \langle m_1\theta_0^{\boxtimes}|_2 \otimes |0\rangle \langle 0|_3 \right) \otimes \left(|m_1\theta_0^{\boxtimes}\rangle \langle m_1\theta_0^{\boxtimes}|_4 \otimes |0\rangle \langle 0|_5 \right) & \text{if } \hat{x}_1 \neq x_1. \end{cases} \quad (59)$$

$$x_2 \oplus x_3 = \hat{x}_1 \quad x_4 \oplus x_5 = \hat{x}_1$$

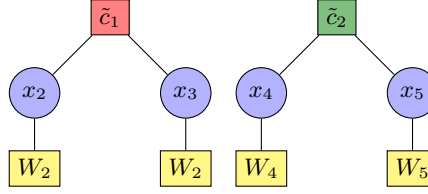


FIG. 7. The reduced factor graph after estimating bit 1 to be \hat{x}_1 .

Lemma 4. Let $C := (I_2)_1 \otimes CNOT_{2 \rightarrow 3} \otimes CNOT_{4 \rightarrow 5}$ and $|\Gamma_{\hat{x}_1}\rangle := \cos \frac{\theta_0^{\otimes}}{2} |00\rangle + (-1)^{\hat{x}_1} \sin \frac{\theta_0^{\otimes}}{2} |11\rangle$. Then

$$C \tilde{\rho}_{\pm, b}^{(m_1)} C^\dagger = \begin{cases} \frac{1}{P_{\text{succ}, 1}^{\text{BPQM}}} |m_1\theta\rangle \langle m_1\theta|_1 \otimes [W \boxtimes W](\hat{x}_1)_{23} \otimes [W \boxtimes W](\hat{x}_1)_{45} \\ + \frac{p_0^2}{P_{\text{succ}, 1}^{\text{BPQM}}} [0.5(1 + \sin \varphi_{00}^{\otimes}) - 1] |m_1\theta\rangle \langle m_1\theta|_1 \otimes |\Gamma_{\hat{x}_1}\rangle \langle \Gamma_{\hat{x}_1}|_{23} \otimes |\Gamma_{\hat{x}_1}\rangle \langle \Gamma_{\hat{x}_1}|_{45} & \text{if } \hat{x}_1 = x_1, \\ |m_1\theta\rangle \langle m_1\theta|_1 \otimes |\Gamma_{\hat{x}_1}\rangle \langle \Gamma_{\hat{x}_1}|_{23} \otimes |\Gamma_{\hat{x}_1}\rangle \langle \Gamma_{\hat{x}_1}|_{45} & \text{if } \hat{x}_1 \neq x_1. \end{cases} \quad (60)$$

Proof. We know from the definition of the factor node convolution operation of BPQM that

$$\begin{aligned} & C (|m_1\theta\rangle \langle m_1\theta|_1 \otimes [W \boxtimes W](\hat{x}_1)_{23} \otimes [W \boxtimes W](\hat{x}_1)_{45}) C^\dagger \\ &= |m_1\theta\rangle \langle m_1\theta|_1 \otimes \left(\sum_{j \in \{0, 1\}} p_j |m_1\theta_j^{\otimes}\rangle \langle m_1\theta_j^{\otimes}|_2 \otimes |j\rangle \langle j|_3 \right) \otimes \left(\sum_{k \in \{0, 1\}} p_k |m_1\theta_k^{\otimes}\rangle \langle m_1\theta_k^{\otimes}|_4 \otimes |k\rangle \langle k|_5 \right) \quad (61) \\ &= \rho_{m_1, b}. \quad (62) \end{aligned}$$

This in turn implies that $C \rho_{m_1, b} C^\dagger = |m_1\theta\rangle \langle m_1\theta|_1 \otimes [W \boxtimes W](\hat{x}_1)_{23} \otimes [W \boxtimes W](\hat{x}_1)_{45}$. Ignoring the first qubit and the constant factor for simplicity, observe that

$$\begin{aligned} \tilde{\rho}_{\pm, b}^{(m_1)} \Big|_{\hat{x}_1 = x_1} &= \sum_{j, k \in \{0, 1\}^2} p_j p_k \left(\left| \langle m_1 | \pm \varphi_{jk}^{\otimes} \rangle \right|^2 - 1 + 1 \right) \left(|m_1\theta_j^{\otimes}\rangle \langle m_1\theta_j^{\otimes}|_2 \otimes |j\rangle \langle j|_3 \right) \otimes \left(|m_1\theta_k^{\otimes}\rangle \langle m_1\theta_k^{\otimes}|_4 \otimes |k\rangle \langle k|_5 \right) \quad (63) \\ &= \rho_{m_1, b} + p_0^2 [0.5(1 + \sin \varphi_{00}^{\otimes}) - 1] \left(|m_1\theta_0^{\otimes}\rangle \langle m_1\theta_0^{\otimes}|_2 \otimes |0\rangle \langle 0|_3 \right) \otimes \left(|m_1\theta_0^{\otimes}\rangle \langle m_1\theta_0^{\otimes}|_4 \otimes |0\rangle \langle 0|_5 \right). \quad (64) \end{aligned}$$

We have used the fact that except when $j = k = 0$, assuming $\hat{x}_1 = x_1$, $\langle m_1 | \pm \varphi_{jk}^{\otimes} \rangle = \langle m_1 | m_1 \varphi_{jk}^{\otimes} \rangle = \langle m_1 | m_1 \rangle = 1$. Finally, using $CNOT_{2 \rightarrow 3} (|m_1\theta_0^{\otimes}\rangle_2 \otimes |0\rangle_3) = |\Gamma_{\hat{x}_1}\rangle$, the result follows for both cases $\hat{x}_1 = x_1$ and $\hat{x}_1 \neq x_1$. \blacksquare

Therefore, after reversing the operations of BPQM for bit x_1 , the 5-qubit system is in the state

$$\tilde{\rho}_{m_1, a} = P_{\text{succ}, 1}^{\text{BPQM}} \cdot C \tilde{\rho}_{\pm, b}^{(m_1)} \Big|_{\hat{x}_1 = x_1} C^\dagger + \left(1 - P_{\text{succ}, 1}^{\text{BPQM}} \right) \cdot C \tilde{\rho}_{\pm, b}^{(m_1)} \Big|_{\hat{x}_1 \neq x_1} C^\dagger \quad (65)$$

$$\begin{aligned} &= |m_1\theta\rangle \langle m_1\theta|_1 \otimes [W \boxtimes W](\hat{x}_1)_{23} \otimes [W \boxtimes W](\hat{x}_1)_{45} \\ &+ p_0^2 [0.5(1 + \sin \varphi_{00}^{\otimes}) - 1] |m_1\theta\rangle \langle m_1\theta|_1 \otimes |\Gamma_{\hat{x}_1}\rangle \langle \Gamma_{\hat{x}_1}|_{23} \otimes |\Gamma_{\hat{x}_1}\rangle \langle \Gamma_{\hat{x}_1}|_{45} \\ &+ \left(1 - P_{\text{succ}, 1}^{\text{BPQM}} \right) \cdot |m_1\theta\rangle \langle m_1\theta|_1 \otimes |\Gamma_{\hat{x}_1}\rangle \langle \Gamma_{\hat{x}_1}|_{23} \otimes |\Gamma_{\hat{x}_1}\rangle \langle \Gamma_{\hat{x}_1}|_{45} \quad (66) \end{aligned}$$

$$= |m_1\theta\rangle \langle m_1\theta|_1 \otimes [W \boxtimes W](\hat{x}_1)_{23} \otimes [W \boxtimes W](\hat{x}_1)_{45}, \quad (67)$$

since $P_{\text{succ}, 1}^{\text{BPQM}} = p_0^2 \cdot 0.5(1 + \sin \varphi_{00}^{\otimes}) + (1 - p_0^2)$.

At this point, we have decoded $\hat{x}_1 = 0$ if $m_1 = +$ and $\hat{x}_1 = 1$ if $m_1 = -$. We can absorb the value of \hat{x}_1 in the FG by updating the parity checks c_1 and c_2 to impose $x_2 \oplus x_3 = \hat{x}_1$ and $x_4 \oplus x_5 = \hat{x}_1$, respectively. Now we have two disjoint FGs as shown in Fig. 7. It suffices to decode x_2 and x_4 since $\hat{x}_3 = \hat{x}_2 \oplus \hat{x}_1$ and $\hat{x}_5 = \hat{x}_4 \oplus \hat{x}_1$. Also, due to symmetry, it suffices to analyze the success probability of decoding x_2 (resp. x_4) and x_3 (resp. x_5). For this reduced

FG, we need to split $\tilde{\rho}_{m_1,a}$ into two density matrices corresponding to the hypotheses $x_2 = 0$ and $x_2 = 1$. If we revisit the density matrices $\rho_1^{(0)}$ and $\rho_1^{(1)}$, we observe that the 5-qubit system at the channel output is exactly $\frac{1}{2}\rho_1^{(0)} + \frac{1}{2}\rho_1^{(1)}$. Hence, for x_2 , we accordingly split $[W \boxtimes W](\hat{x}_1)_{23}$ in $\tilde{\rho}_{m_1,a}$ and arrive at the two hypotheses states

$$\tilde{\Phi}_{x_2=\hat{x}_1}(\hat{x}_1) = |m_1\theta\rangle\langle m_1\theta|_2 \otimes |\theta\rangle\langle\theta|_3 \otimes [W \boxtimes W](\hat{x}_1)_{45}, \quad (68)$$

$$\tilde{\Phi}_{x_2 \neq \hat{x}_1}(\hat{x}_1) = |-m_1\theta\rangle\langle -m_1\theta|_2 \otimes |-\theta\rangle\langle -\theta|_3 \otimes [W \boxtimes W](\hat{x}_1)_{45}. \quad (69)$$

We can deterministically apply $Z^{\hat{x}_1}$ to system 2 in order to map this into the following state discrimination problem:

$$\Phi_{\pm}(\hat{x}_1) = |\pm\theta\rangle\langle\pm\theta|_2 \otimes |\pm\theta\rangle\langle\pm\theta|_3 \otimes [W \boxtimes W](\hat{x}_1)_{45}, \quad (70)$$

where $\pm \equiv (-1)^{x_2-\hat{x}_1}$. Clearly, we can process systems 2 and 3 alone to decide x_2 , and similarly systems 4 and 5 alone to decide x_4 . It is also clear that by performing the variable node operation $U_{\circledast}(\theta, \theta)$, we compress all the information into system 2, i.e., produce $|\pm\theta^*\rangle\langle\pm\theta^*|_2 \otimes |0\rangle\langle 0|_3$, which can then be optimally distinguished by measuring in the X -basis. This agrees with the definition of node operations in BPQM as well because now the factor node \tilde{c}_1 in Fig. 7 has degree 2, and hence the optimal processing is to perform the variable node convolution between qubits 2 and 3. We can incorporate the operation $Z^{\hat{x}_1}$ into BPQM by performing $U_{\circledast}(m_1\theta, \theta)$ on systems 2 and 3 (and similarly on systems 4 and 5). Although $U_{\circledast}(m_1\theta, \theta) \neq U_{\circledast}(\theta, \theta) \cdot (Z^{\hat{x}_1} \otimes I_2)$, the two operations act identically on the states $\tilde{\Phi}_{x_2=\hat{x}_1}(\hat{x}_1)$ and $\tilde{\Phi}_{x_2 \neq \hat{x}_1}(\hat{x}_1)$.

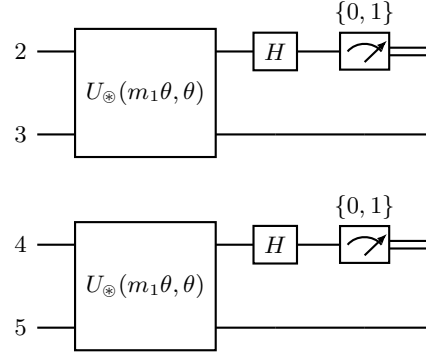


FIG. 8. The circuit performed in BPQM after decoding bit x_1 and reversing the operations performed prior to measurement.

Hence, since the operation in Fig. 8 is optimal (Helstrom) for distinguishing $\tilde{\Phi}_{x_2=\hat{x}_1}(\hat{x}_1)$ and $\tilde{\Phi}_{x_2 \neq \hat{x}_1}(\hat{x}_1)$, we expect the BPQM success probability for decoding $\hat{x}_2 = x_2$ to be

$$\mathbb{P}[\hat{x}_2 = x_2] = \frac{1}{2} + \frac{1}{4} \|\tilde{\Phi}_{x_2=\hat{x}_1}(\hat{x}_1) - \tilde{\Phi}_{x_2 \neq \hat{x}_1}(\hat{x}_1)\|_1 \quad (71)$$

$$= \frac{1}{2} + \frac{1}{4} \|\Phi_+(\hat{x}_1) - \Phi_-(\hat{x}_1)\|_1 \quad (72)$$

$$= \frac{1}{2} + \frac{1}{4} \|(|\theta^*\rangle\langle\theta^*| - |-\theta^*\rangle\langle -\theta^*|)_2 \otimes |0\rangle\langle 0|_3 \otimes [W \boxtimes W](\hat{x}_1)_{45}\|_1 \quad (73)$$

$$= \frac{1}{2} + \frac{1}{4} \cdot \sin \theta^* \|X\|_1 \quad (74)$$

$$= \frac{1 + \sin \theta^*}{2} = \frac{1 + \sqrt{1 - \cos^4 \theta}}{2}. \quad (75)$$

Note that if we had defined the state $\tilde{\rho}_{m_1,a}$ to be conditioned on the cases $\hat{x}_1 = x_1$ and $\hat{x}_1 \neq x_1$ separately, then using a similar calculation as above we would still obtain

$$\mathbb{P}[\hat{x}_2 = x_2] = \mathbb{P}[\hat{x}_1 = x_1] \cdot \mathbb{P}[\hat{x}_2 = x_2 | \hat{x}_1 = x_1] + \mathbb{P}[\hat{x}_1 \neq x_1] \cdot \mathbb{P}[\hat{x}_2 = x_2 | \hat{x}_1 \neq x_1] \quad (76)$$

$$= P_{\text{succ},1}^{\text{BPQM}} \cdot \frac{1}{2} \left(1 + \frac{\sin \theta^*}{P_{\text{succ},1}^{\text{BPQM}}} \right) + \left(1 - P_{\text{succ},1}^{\text{BPQM}} \right) \cdot \frac{1}{2} = \frac{1 + \sin \theta^*}{2}. \quad (77)$$

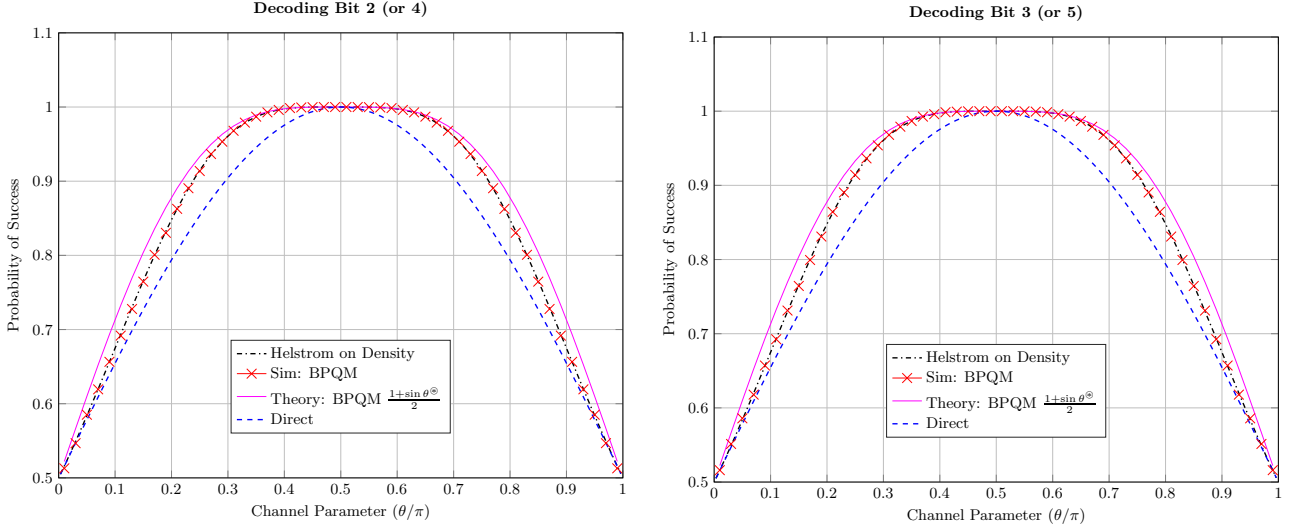


FIG. 9. The success probabilities for decoding the value of x_2 or x_4 (left) and x_3 or x_5 (right) in the 5-bit code. Here, “Helstrom on Density” represents $P_{\text{succ},k}^{\text{Hel}}$ and “Direct” represents the success probability when directly implementing the Helstrom measurement at the channel output on system k , for $k \in \{2, 3, 4, 5\}$. The curves “Sim: BPQM” correspond to a simulation that averaged each data point over 10^5 uniformly random codeword transmissions.

Finally, bits x_3 and x_5 can be estimated simply as $\hat{x}_3 = \hat{x}_2 \oplus \hat{x}_1$ and $\hat{x}_5 = \hat{x}_4 \oplus \hat{x}_1$, without performing any quantum operations. Due to symmetry, the success probabilities for both these bits are the same. Bit 3 is decoded correctly, i.e., $\hat{x}_3 = x_3$, if either $\hat{x}_1 = x_1$ and $\hat{x}_2 = x_2$ or $\hat{x}_1 \neq x_1$ and $\hat{x}_2 \neq x_2$. Hence, we can write

$$\mathbb{P}[\hat{x}_3 = x_3] = \mathbb{P}[\hat{x}_1 = x_1] \cdot \mathbb{P}[\hat{x}_2 = x_2 | \hat{x}_1 = x_1] + \mathbb{P}[\hat{x}_1 \neq x_1] \cdot \mathbb{P}[\hat{x}_2 \neq x_2 | \hat{x}_1 \neq x_1] \quad (78)$$

$$= P_{\text{succ},1}^{\text{BPQM}} \cdot \frac{1}{2} \left(1 + \frac{\sin \theta^*}{P_{\text{succ},1}^{\text{BPQM}}} \right) + \left(1 - P_{\text{succ},1}^{\text{BPQM}} \right) \cdot \frac{1}{2} \quad (79)$$

$$= \frac{1 + \sin \theta^*}{2}. \quad (80)$$

Again, $P_{\text{succ},5}^{\text{Hel}} = P_{\text{succ},3}^{\text{Hel}}$, and these probabilities are plotted in Fig. 9 (right).

We simulated the performance of BPQM by randomly generating 10^5 codewords, passing each of them through 5 independent copies of the pure state channel, and employing the above sequence of unitaries and measurements for decoding all the bits. We plot the empirical performance of BPQM for decoding bit 2 in Fig. 9 (left), along with the predicted theoretical performance above, the performance for directly measuring the second qubit at the channel output, and also the Helstrom success probability $P_{\text{succ},2}^{\text{Hel}}$ for optimally distinguishing $\rho_2^{(0)}$ and $\rho_2^{(1)}$, where

$$\rho_2^{(0)} = |\theta\rangle\langle\theta|_2 \otimes \left[\frac{1}{2} |\theta\rangle\langle\theta|_1 \otimes |\theta\rangle\langle\theta|_3 \otimes [W \boxtimes W](0)_{45} + \frac{1}{2} |-\theta\rangle\langle-\theta|_1 \otimes |-\theta\rangle\langle-\theta|_3 \otimes [W \boxtimes W](1)_{45} \right], \quad (81)$$

$$\rho_2^{(1)} = |-\theta\rangle\langle-\theta|_2 \otimes \left[\frac{1}{2} |\theta\rangle\langle\theta|_1 \otimes |-\theta\rangle\langle-\theta|_3 \otimes [W \boxtimes W](0)_{45} + \frac{1}{2} |-\theta\rangle\langle-\theta|_1 \otimes |\theta\rangle\langle\theta|_3 \otimes [W \boxtimes W](1)_{45} \right]. \quad (82)$$

We observe that BPQM performs significantly better than direct Helstrom measurement of the channel output, as we might expect. Moreover, the performance of BPQM is indistinguishable (up to numerical precision) from that of the Helstrom measurement that optimally distinguishes between $\rho_2^{(0)}$ and $\rho_2^{(1)}$. This suggests that BPQM might be provably optimal for decoding bit 2 as well, even though the measurement for bit 1 rendered the original channel outputs irrecoverable. However, we also notice that the above prediction for the BPQM success probability for decoding bit 2 is relatively higher than even the optimal Helstrom measurement. This indicates that the state discrimination problem for bit 2 discussed above is more ideal than the actual problem in hand. Hence, next we analyze the true state discrimination problem for bit 2 (or 4) and clarify the observed performance in Fig. 9.

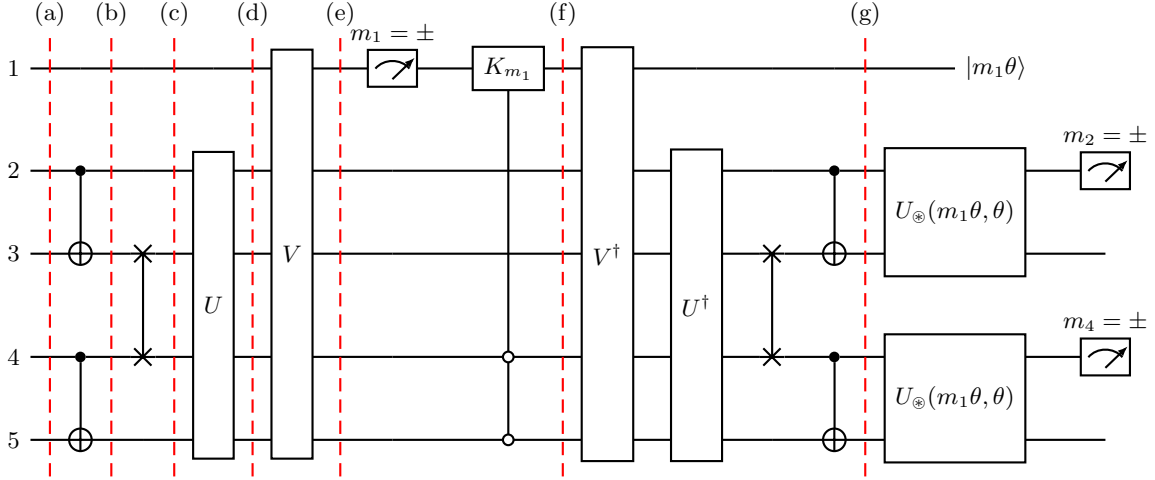


FIG. 10. The full BPQM circuit to decode all bits of the 5-bit code in Fig. 2. The decoded values are related to the measurement results as $m_1 = (-1)^{\hat{x}_1}$, $m_2 = (-1)^{\hat{x}_2}$, $m_4 = (-1)^{\hat{x}_4}$, and $\hat{x}_3 = \hat{x}_1 \oplus \hat{x}_2$, $\hat{x}_5 = \hat{x}_1 \oplus \hat{x}_4$. The open-circled controls indicate that K_{m_1} is coherently controlled by the last two qubits being in the state $|00\rangle_{45}$. The solid line before K_{m_1} indicates that the controlled unitary is applied to the post-measurement state. See Fig. 13 for the full decomposition of this circuit.

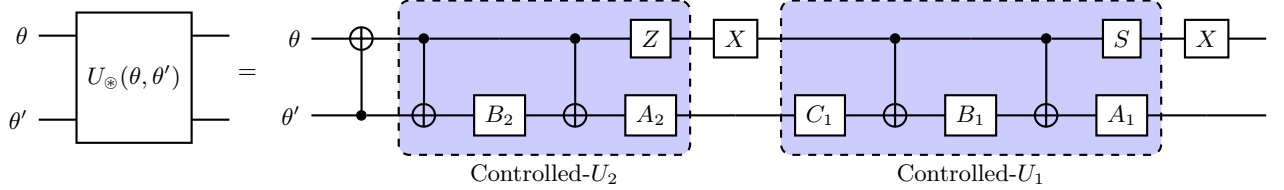


FIG. 11. The circuit decomposition for $U_⊗(\theta, \theta')$, where we set $A_1 := R_y(\gamma_1/2)$, $B_1 := R_y(-\gamma_1/2)R_z(-\pi/2)$, $C_1 := R_z(\pi/2)$, $A_2 := R_z(\pi)R_y(\gamma_2/2)$, $B_2 := R_y(-\gamma_2/2)R_z(-\pi)$, and $S = \sqrt{Z}$ is the phase gate. See Appendix A for calculations and angles γ_1, γ_2 . Note that, for example, $B_2 = R_y(-\gamma_2/2)R_z(-\pi)$ implies that $R_z(-\pi)$ must be applied first, then followed by $R_y(-\gamma_2/2)$.

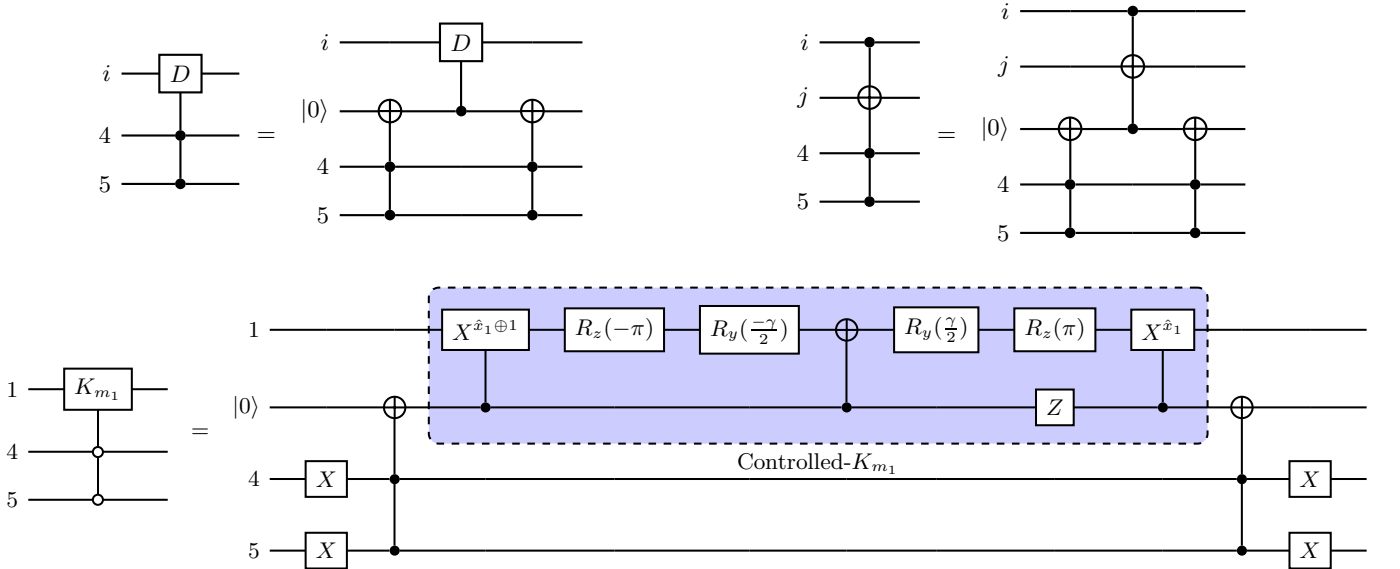


FIG. 12. Decomposition of controlled gates using Toffoli (or CCZ) gates and an ancilla [28, Fig. 4.10], where $i, j \in \{1, 2, 3\}$ and $D \in \{A_1, B_1, C_1, A_2, B_2, S\}$ as appropriate. The top two identities can be used to implement each of the doubly-controlled $U_⊗(\theta, \theta')$ appearing in Fig. 13 by applying doubly-controlled versions of the components of $U_⊗(\theta, \theta')$ in Fig. 11. Note that $m_1 = (-1)^{\hat{x}_1}$ is the result of estimating x_1 to be $\hat{x}_1 \in \{0, 1\}$. See Appendix A for the relevant calculations and the angle γ .

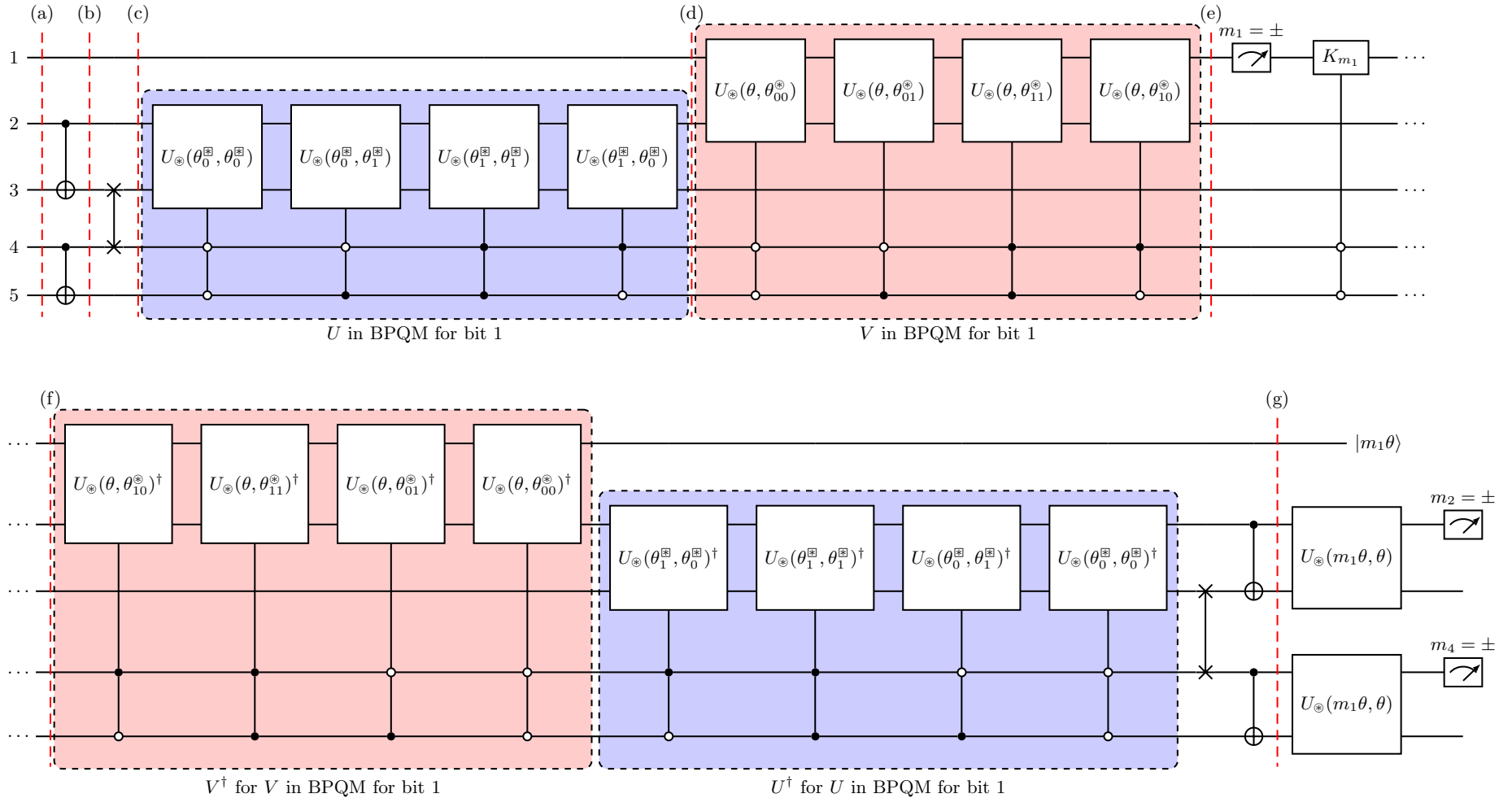


FIG. 13. Full decomposition of the BPQM circuit in Fig. 10. The variable node unitaries $U_*(\theta, \theta')$ are decomposed in Fig. 11. The two-qubit-controlled coherent versions of these unitaries as well as the single-qubit rotation K_{m_1} , which is a function of the measurement result m_1 , are decomposed in Fig. 12.

C. Analysis of BPQM Optimality for Decoding Bit 2 (or 4)

At the channel output, it is clear that the optimal strategy to decode bit 2 is to perform the Helstrom measurement that distinguishes between $\rho_2^{(0)}$ and $\rho_2^{(1)}$. However, since we performed BPQM operations to decode bit 1 first, these two density matrices would have evolved through that process. Therefore, the correct analysis is to derive the resulting states and then subject them to the BPQM strategy for decoding bit 2 that was discussed above. For simplicity, we only track the density matrix $\rho_2^{(0)}$ through the different stages in Fig. 10 (or Fig. 13). The corresponding states for $\rho_2^{(1)}$ can easily be ascertained from these. It will be convenient to express

$$\frac{1}{2} |\theta\rangle \langle \theta|_2 \otimes |\theta\rangle \langle \theta|_3 = [W \boxtimes W](0)_{23} - \frac{1}{2} |-\theta\rangle \langle -\theta|_2 \otimes |-\theta\rangle \langle -\theta|_3, \quad (83)$$

$$\frac{1}{2} |\theta\rangle \langle \theta|_2 \otimes |-\theta\rangle \langle -\theta|_3 = [W \boxtimes W](1)_{23} - \frac{1}{2} |-\theta\rangle \langle -\theta|_2 \otimes |\theta\rangle \langle \theta|_3. \quad (84)$$

For brevity, we will use the notation $\text{CX}_{ij} := \text{CNOT}_{i \rightarrow j}$ and $\text{Swap}_{34} := \text{CX}_{34} \text{CX}_{43} \text{CX}_{34}$. Then we can write

$$\rho_{2,a}^{(0)} = \frac{1}{2} |\theta\rangle \langle \theta|_1 \otimes |\theta\rangle \langle \theta|_2 \otimes |\theta\rangle \langle \theta|_3 \otimes [W \boxtimes W](0)_{45} + \frac{1}{2} |-\theta\rangle \langle -\theta|_1 \otimes |\theta\rangle \langle \theta|_2 \otimes |-\theta\rangle \langle -\theta|_3 \otimes [W \boxtimes W](1)_{45}, \quad (85)$$

$$\begin{aligned} \rho_{2,b}^{(0)} = & |\theta\rangle \langle \theta|_1 \otimes \left[\sum_{j=0,1} p_j |\theta_j^{\boxtimes}\rangle \langle \theta_j^{\boxtimes}|_2 \otimes |j\rangle \langle j|_3 - \frac{1}{2} \text{CX}_{23} |-\theta, -\theta\rangle \langle -\theta, -\theta|_{23} \text{CX}_{23} \right] \otimes \left[\sum_{k=0,1} p_k |\theta_k^{\boxtimes}\rangle \langle \theta_k^{\boxtimes}|_4 \otimes |k\rangle \langle k|_5 \right] \\ & + |-\theta\rangle \langle -\theta|_1 \otimes \left[\sum_{j=0,1} p_j |-\theta_j^{\boxtimes}\rangle \langle -\theta_j^{\boxtimes}|_2 \otimes |j\rangle \langle j|_3 - \frac{1}{2} \text{CX}_{23} |-\theta, \theta\rangle \langle -\theta, \theta|_{23} \text{CX}_{23} \right] \\ & \quad \otimes \left[\sum_{k=0,1} p_k |-\theta_k^{\boxtimes}\rangle \langle -\theta_k^{\boxtimes}|_4 \otimes |k\rangle \langle k|_5 \right], \end{aligned} \quad (86)$$

$$\begin{aligned} \rho_{2,c}^{(0)} = & |\theta\rangle \langle \theta|_1 \otimes \sum_{j,k \in \{0,1\}^2} p_j p_k |\theta_j^{\boxtimes}\rangle \langle \theta_j^{\boxtimes}|_2 \otimes |\theta_k^{\boxtimes}\rangle \langle \theta_k^{\boxtimes}|_3 \otimes |j\rangle \langle j|_4 \otimes |k\rangle \langle k|_5 \\ & - \frac{1}{2} |\theta\rangle \langle \theta|_1 \otimes \text{Swap}_{34} \left[\text{CX}_{23} |-\theta, -\theta\rangle \langle -\theta, -\theta|_{23} \text{CX}_{23} \otimes \sum_{k=0,1} p_k |\theta_k^{\boxtimes}\rangle \langle \theta_k^{\boxtimes}|_4 \otimes |k\rangle \langle k|_5 \right] \text{Swap}_{34} \\ & + |-\theta\rangle \langle -\theta|_1 \otimes \sum_{j,k \in \{0,1\}^2} p_j p_k |-\theta_j^{\boxtimes}\rangle \langle -\theta_j^{\boxtimes}|_2 \otimes |-\theta_k^{\boxtimes}\rangle \langle -\theta_k^{\boxtimes}|_3 \otimes |j\rangle \langle j|_4 \otimes |k\rangle \langle k|_5 \\ & - \frac{1}{2} |-\theta\rangle \langle -\theta|_1 \otimes \text{Swap}_{34} \left[\text{CX}_{23} |-\theta, \theta\rangle \langle -\theta, \theta|_{23} \text{CX}_{23} \otimes \sum_{k=0,1} p_k |-\theta_k^{\boxtimes}\rangle \langle -\theta_k^{\boxtimes}|_4 \otimes |k\rangle \langle k|_5 \right] \text{Swap}_{34}, \end{aligned} \quad (87)$$

$$\begin{aligned} \rho_{2,e}^{(0)} = & \sum_{j,k \in \{0,1\}^2} p_j p_k |\varphi_{jk}^{\circledast}\rangle \langle \varphi_{jk}^{\circledast}|_1 \otimes |0\rangle \langle 0|_2 \otimes |0\rangle \langle 0|_3 \otimes |jk\rangle \langle jk|_{45} \\ & + \sum_{j,k \in \{0,1\}^2} p_j p_k |-\varphi_{jk}^{\circledast}\rangle \langle -\varphi_{jk}^{\circledast}|_1 \otimes |0\rangle \langle 0|_2 \otimes |0\rangle \langle 0|_3 \otimes |jk\rangle \langle jk|_{45} \\ & - \frac{1}{2} VU \left\{ |\theta\rangle \langle \theta|_1 \otimes \text{Swap}_{34} \left[\text{CX}_{23} |-\theta, -\theta\rangle \langle -\theta, -\theta|_{23} \text{CX}_{23} \otimes \sum_{k=0,1} p_k |\theta_k^{\boxtimes}\rangle \langle \theta_k^{\boxtimes}|_4 \otimes |k\rangle \langle k|_5 \right] \text{Swap}_{34} \right. \\ & \left. + |-\theta\rangle \langle -\theta|_1 \otimes \text{Swap}_{34} \left[\text{CX}_{23} |-\theta, \theta\rangle \langle -\theta, \theta|_{23} \text{CX}_{23} \otimes \sum_{k=0,1} p_k |-\theta_k^{\boxtimes}\rangle \langle -\theta_k^{\boxtimes}|_4 \otimes |k\rangle \langle k|_5 \right] \text{Swap}_{34} \right\} U^{\dagger} V^{\dagger}. \end{aligned} \quad (88)$$

Next we make an X -basis measurement on the first qubit, and for convenience we assume that the measurement result is $m_1 = +$. The analysis for $m_1 = -$ is very similar and follows by symmetry. We verified numerically that $\text{Tr} [|+\rangle \langle +|_1 \cdot \rho_{2,e}^{(0)}] = 0.5$, which we might intuitively expect since $\rho_{2,e}^{(0)}$ is the density matrix for $x_2 = 0$ and x_2 is

independent from x_1 . Since $m_1 = +$, we follow the measurement with the conditional rotation M_+ in (55) to obtain

$$\begin{aligned} \Phi_{2,m_1=+}^{(0)} = & \frac{1}{0.5} \left[\sum_{j,k \in \{0,1\}^2} p_j p_k |\langle +|\varphi_{jk}^{\circledast} \rangle|^2 |\varphi_{jk}^{\circledast} \rangle \langle \varphi_{jk}^{\circledast} |_1 \otimes |0\rangle \langle 0|_2 \otimes |0\rangle \langle 0|_3 \otimes |jk\rangle \langle jk|_{45} \right. \\ & + \frac{p_0^2(1 - \sin \varphi_{00}^{\circledast})}{2} |\varphi_{00}^{\circledast} \rangle \langle \varphi_{00}^{\circledast}| \otimes |0\rangle \langle 0|_2 \otimes |0\rangle \langle 0|_3 \otimes |00\rangle \langle 00|_{45} \\ & \left. - \frac{1}{2} M_+ |+\rangle \langle +|_1 V U \Lambda_2^{(0)} U^\dagger V^\dagger |+\rangle \langle +|_1 M_+^\dagger \right], \end{aligned} \quad (89)$$

$$\begin{aligned} \Lambda_2^{(0)} := & |\theta\rangle \langle \theta|_1 \otimes \text{Swap}_{34} \left[\text{CX}_{23} |-\theta, -\theta\rangle \langle -\theta, -\theta|_{23} \text{CX}_{23} \otimes \sum_{k=0,1} p_k |\theta_k^{\boxtimes} \rangle \langle \theta_k^{\boxtimes}|_4 \otimes |k\rangle \langle k|_5 \right] \text{Swap}_{34} \\ & + |-\theta\rangle \langle -\theta|_1 \otimes \text{Swap}_{34} \left[\text{CX}_{23} |-\theta, \theta\rangle \langle -\theta, \theta|_{23} \text{CX}_{23} \otimes \sum_{k=0,1} p_k |-\theta_k^{\boxtimes} \rangle \langle -\theta_k^{\boxtimes}|_4 \otimes |k\rangle \langle k|_5 \right] \text{Swap}_{34}. \end{aligned} \quad (90)$$

This is the state at stage (f) in Fig. 10. Hence, for $x_2 = 0$, the density matrix we have when $\hat{x}_1 = 0$ and we reverse the BPQM operations on $\Phi_{2,m_1=+}^{(0)}$ is

$$\begin{aligned} \tilde{\rho}_{2,m_1=+}^{(0)} = & \frac{1}{0.5} \left[|\theta\rangle \langle \theta|_1 \otimes [W \boxtimes W](0)_{23} \otimes [W \boxtimes W](0)_{45} \right. \\ & \left. - \frac{1}{2} \text{CX}_{23} \text{CX}_{45} \text{Swap}_{34} U^\dagger V^\dagger M_+ |+\rangle \langle +|_1 V U \Lambda_2^{(0)} U^\dagger V^\dagger |+\rangle \langle +|_1 M_+^\dagger V U \text{Swap}_{34} \text{CX}_{45} \text{CX}_{23} \right]. \end{aligned} \quad (91)$$

This is the state at stage (g) in Fig. 10. So, this is the actual density matrix that BPQM encounters for $x_2 = 0$ after having estimated $\hat{x}_1 = 0$. When compared with the earlier analysis, we observe numerically that this is close to $\tilde{\Phi}_{x_2=\hat{x}_1}(\hat{x}_1)$ but is not exactly the same. For example, when $\theta = 0.1\pi$ we find that $\|\tilde{\rho}_{2,m_1=+}^{(0)} - \tilde{\Phi}_{x_2=0}(0)\|_{\text{Fro}} = 0.0542$, where ‘‘Fro’’ denotes the Frobenius norm, and only two of the distinct entries differ (slightly). Similarly,

$$\begin{aligned} \tilde{\rho}_{2,m_1=+}^{(1)} = & \frac{1}{0.5} \left[|\theta\rangle \langle \theta|_1 \otimes [W \boxtimes W](0)_{23} \otimes [W \boxtimes W](0)_{45} \right. \\ & \left. - \frac{1}{2} \text{CX}_{23} \text{CX}_{45} \text{Swap}_{34} U^\dagger V^\dagger M_+ |+\rangle \langle +|_1 V U \Lambda_2^{(1)} U^\dagger V^\dagger |+\rangle \langle +|_1 M_+^\dagger V U \text{Swap}_{34} \text{CX}_{45} \text{CX}_{23} \right], \end{aligned} \quad (92)$$

$$\begin{aligned} \Lambda_2^{(1)} := & |\theta\rangle \langle \theta|_1 \otimes \text{Swap}_{34} \left[\text{CX}_{23} |\theta, \theta\rangle \langle \theta, \theta|_{23} \text{CX}_{23} \otimes \sum_{k=0,1} p_k |\theta_k^{\boxtimes} \rangle \langle \theta_k^{\boxtimes}|_4 \otimes |k\rangle \langle k|_5 \right] \text{Swap}_{34} \\ & + |-\theta\rangle \langle -\theta|_1 \otimes \text{Swap}_{34} \left[\text{CX}_{23} |\theta, -\theta\rangle \langle \theta, -\theta|_{23} \text{CX}_{23} \otimes \sum_{k=0,1} p_k |-\theta_k^{\boxtimes} \rangle \langle -\theta_k^{\boxtimes}|_4 \otimes |k\rangle \langle k|_5 \right] \text{Swap}_{34}. \end{aligned} \quad (93)$$

However, most importantly, we observe that $\frac{1}{2}\tilde{\rho}_{2,m_1=+}^{(0)} + \frac{1}{2}\tilde{\rho}_{2,m_1=+}^{(1)} = \frac{1}{2}\tilde{\Phi}_{x_2=0}(0) + \frac{1}{2}\tilde{\Phi}_{x_2=1}(0)$. This explains that while the full density matrix $\tilde{\rho}_{m_1,a}$ was correct, we had split it incorrectly to arrive at the two hypotheses $\tilde{\Phi}_{x_2=\hat{x}_1}(\hat{x}_1)$ and $\tilde{\Phi}_{x_2 \neq \hat{x}_1}(\hat{x}_1)$. Now, the Helstrom measurement that optimally distinguishes between $\tilde{\rho}_{2,m_1=+}^{(0)}$ and $\tilde{\rho}_{2,m_1=+}^{(1)}$ only depends on

$$\tilde{\rho}_{2,m_1=+}^{(0)} - \tilde{\rho}_{2,m_1=+}^{(1)} = A \left[\Lambda_2^{(1)} - \Lambda_2^{(0)} \right] A^\dagger, \quad A := \text{CX}_{23} \text{CX}_{45} \text{Swap}_{34} U^\dagger V^\dagger M_+ |+\rangle \langle +|_1 V U. \quad (94)$$

By symmetry of $m_1 = +$ and $m_1 = -$, the optimal success probability to decide bit 2 is given by

$$P_{\text{succ},2}^{\text{Hel}} = \frac{1}{2} + \frac{1}{4} \left\| \tilde{\rho}_{2,m_1=+}^{(0)} - \tilde{\rho}_{2,m_1=+}^{(1)} \right\|_1 = \frac{1}{2} + \frac{1}{4} \left\| A \left[\Lambda_2^{(1)} - \Lambda_2^{(0)} \right] A^\dagger \right\|_1 = \frac{1}{2} + \frac{1}{4} \left\| L \left(\rho_2^{(0)} - \rho_2^{(1)} \right) L^\dagger \right\|_1, \quad (95)$$

$$L := \text{CX}_{23} \text{CX}_{45} \text{Swap}_{34} U^\dagger V^\dagger M_+ \frac{|+\rangle \langle +|_1}{\sqrt{0.5}} V U \text{Swap}_{34} \text{CX}_{45} \text{CX}_{23}. \quad (96)$$

Since L is not unitary, we cannot directly apply the unitary invariance of the trace norm to conclude that there is no degradation in performance when compared to optimally distinguishing $\rho_2^{(0)}$ and $\rho_2^{(1)}$ at the channel output.

However, we observe numerically (even up to 12 significant digits) that the operations in L indeed ensure that $\left\| L \left(\rho_2^{(0)} - \rho_2^{(1)} \right) L^\dagger \right\|_1 = \left\| \rho_2^{(0)} - \rho_2^{(1)} \right\|_1$. Moreover, we also observe that the BPQM operations for bit 2 given in Fig. 8 achieve the same success probability, i.e., using the notation $\pm \equiv (-1)^{x_2}$ we have

$$P_{\text{succ},2}^{\text{BPQM}} = \text{Tr} \left[U_{\circledast}(m_1 \theta, \theta) \tilde{\rho}_{2,m_1}^{(x_2)} U_{\circledast}(m_1 \theta, \theta)^\dagger \cdot |\pm\rangle \langle \pm|_2 \right] \quad (97)$$

$$= \frac{1}{2} + \frac{1}{4} \left\| L \left(\rho_2^{(0)} - \rho_2^{(1)} \right) L^\dagger \right\|_1 \quad (98)$$

$$= \frac{1}{2} + \frac{1}{4} \left\| \rho_2^{(0)} - \rho_2^{(1)} \right\|_1 \quad (99)$$

$$= P_{\text{succ},2}^{\text{Hel}}. \quad (100)$$

Finally, the simulation results in Fig. 14 clearly show that the overall block error rate of BPQM coincides with that of the quantum optimal joint Helstrom limit. It remains open to rigorously prove all of these observations.

D. Overall Performance of BPQM

We can calculate the probability that the full codeword \underline{x} is decoded correctly as

$$\mathbb{P}[\hat{\underline{x}} = \underline{x}] = \mathbb{P}[\hat{x}_1 = x_1] \cdot \mathbb{P}[\hat{x}_2 = x_2 | \hat{x}_1 = x_1] \cdot \mathbb{P}[\hat{x}_4 = x_4 | \hat{x}_1 = x_1] = P_{\text{succ},1}^{\text{Hel}} \left(\frac{1}{2} + \frac{1}{4P_{\text{succ},1}^{\text{Hel}}} \left\| A \left[\tilde{\Lambda}_2^{(1)} - \tilde{\Lambda}_2^{(0)} \right] A^\dagger \right\|_1 \right)^2, \quad (101)$$

where $\tilde{\Lambda}_2^{(0)}$ and $\tilde{\Lambda}_2^{(1)}$ only contain the first (resp. second) term of $\Lambda_2^{(0)}$ and $\Lambda_2^{(1)}$ respectively, if $x_1 = 0$ (resp. $x_1 = 1$), since we have assumed that $\hat{x}_1 = x_1$. The BPQM success probabilities for all bits as well as the simulated estimation of this overall BPQM block success probability are plotted in Fig. 14 (left). For convenience these performance curves are also plotted in a log-log scale along with the codeword Helstrom limit (right). The plots show that even though BPQM is optimal for bits x_2 through x_5 , it still performs slightly poorly when compared to the performance for x_1 . This might be attributed to the fact that in the chosen parity-check matrix, bit x_1 is involved in both checks whereas the other bits are involved in exactly one of the two checks.

Remark 5. *The above analyses demonstrate that even though the measurement for each bit is irreversible, BPQM still decides each bit optimally in this 5-bit example code. In particular, the order in which the bits are decoded does not seem to affect the performance. This needs to be studied further and we need to analyze if BPQM always achieves the codeword Helstrom limit for all codes with tree factor graphs. We emphasize that, while in classical BP there is no question of ordering and one makes hard decisions on all the bits simultaneously after several BP iterations, it appears that quantum BP always has a sequential nature due to the unitarity of operations and the no-cloning theorem. This resembles “successive-cancellation” type decoders more than BP. Due to these facts, we expect that extending classical ideas for analyzing BP, such as density evolution [9], will be challenging in the quantum setting.*

In connection to this, Renes has recently developed a precise notion of duality between channels, and shown that classical channels need to be embedded in CQ channels in order to define their duals [30]. An interesting fact that follows from this framework is that the dual of the pure-state channel is the classical binary symmetric channel (BSC). Since we know that density evolution is a well-defined analysis technique for BP on BSCs, albeit sophisticated, it will be interesting to see if duality allows one to borrow from this literature and analyze BPQM on pure-state channels.

Finally, as briefly discussed in the introduction, we compare the error rates of the following strategies:

- (a) collective (optimal) Helstrom measurement on all channel outputs corresponding to the transmitted codeword,
- (b) BPQM on all channel outputs corresponding to the transmitted codeword,
- (c) symbol-by-symbol (optimal) Helstrom measurement followed by classical (optimal) block-MAP decoding, and
- (d) symbol-by-symbol (optimal) Helstrom measurement followed by classical BP decoding.

For strategy (a), we calculated the performance of the collective Helstrom measurement using the Yuen-Kennedy-Lax (YKL) conditions [18] as discussed, for example, in [19]. Note that, for the last two schemes, classical processing is performed essentially for the BSC induced by measuring each qubit output by the pure-state channel. We had plotted the block error rates earlier in Fig. 1, and we plot bit and block error rates in Fig. 14. The mean photon number per mode, N , relates to the pure-state channel parameter θ as $\cos \theta = e^{-2N}$ (e.g., see [13] for more information on this quantity). We make the following observations from these performance curves.

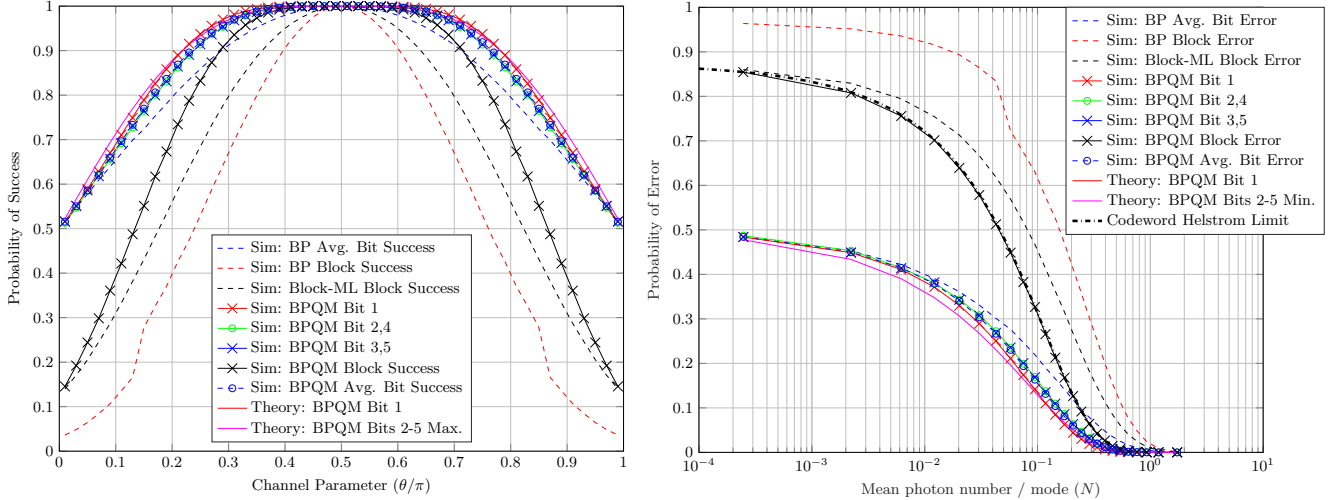


FIG. 14. (left) The BPQM success probabilities for decoding each bit and its overall performance for the 5-bit code, the theoretical BPQM/Helstrom success rate for bit 1, the initial theoretical prediction of $0.5(1 + \sin \theta^\circ)$ for BPQM for bits 2-5, and the performance of BP and block-ML when applied to the directly measured channel outputs. (right) The same curves on the left along with the joint (codeword) Helstrom limit plotted against the mean photon number per mode N ($\cos \theta = e^{-2N}$). Each data point in all simulation curves was obtained by averaging over 10^5 uniformly random codeword transmissions.

1. The block error rates are in increasing order from strategy (a) to (d), as we might expect. Even though classical BP is performed on a tree FG here, it only implements bit-MAP decoding and not block-MAP decoding. This is why it performs worse than block-ML (i.e., block-MAP with uniform prior on codewords) in this case.
2. BPQM performs strictly better than symbol-by-symbol optimal detection followed by classical MAP decoding. This gives a clear demonstration that if one physically constructs a receiver for BPQM, then it will be the best known physically realizable receiver for the pure-state channel. For example, the *Dolinar receiver* [13, 16] realizes only strategy (c). One can use our circuits to make such a physical realization.
3. *BPQM performs as well as the quantum optimal collective Helstrom measurement on the outputs of the channel.* This lends evidence to the conclusion that by passing *quantum* messages, BPQM is able to behave like a collective measurement while still making only single-qubit Pauli measurements during the process. However, more careful analysis is required to characterize this in general for, say, the family of codes with tree FGs.
4. As a first self-consistency check, observe that the block-ML curve asymptotes at roughly 0.875 for low mean photon numbers per mode. This is because, in this regime, the BSC induced by the symbol-by-symbol measurement essentially has a bit-flip rate of 0.5. Therefore, block-ML computes a posterior that is almost uniform on all codewords, and thus the block success probability is $1/|\mathcal{C}| = 1/8 = 0.125$.
5. As another self-consistency check, note that the BP curve asymptotes at roughly $(1 - 1/32) = 0.9688$ for low mean photon numbers per mode. Since BP performs bit-MAP on this FG, and the induced BSC in this regime flips bits at a rate of almost 0.5, BP essentially picks each bit uniformly at random, thereby returning a vector that is uniformly at random out of all the possible $2^5 = 32$ vectors of length 5.

VI. CONCLUSION

This paper began by reviewing classical belief-propagation, which is an algorithm to efficiently perform statistical inference by computing posterior marginal distributions of the involved variables. Then, it discusses an induced channel perspective of understanding the action of classical BP, and generalizes it to the quantum case following Renes [21]. Next, we use an example 5-bit code to understand the recently introduced belief-propagation algorithm with quantum messages (BPQM) algorithm. Since the action of BPQM after decoding the first bit is somewhat ambiguous in the original BPQM paper [21], we introduce a perspective that provides a nice interpretation of BPQM. We also provide a detailed analysis of the density matrices involved in BPQM, and show that BPQM is optimal for

decoding all bits despite performing irreversible (single-qubit) measurements along the way. Finally, we calculate the BPQM success probabilities for all bits and verify empirically that it performs as well as Helstrom's optimal joint measurement strategy for quantum systems.

This is the first practically feasible decoder that can be used to decode the classical-quantum polar codes on the pure state channel. Although CQ polar codes are known to achieve capacity on CQ channels when paired with a quantum successive cancellation decoder [13, 27], it is not clear whether BPQM retains this property. This is because the quantum optimal nature of BPQM, at least for this 5-bit code, does not immediately imply that it must also be a capacity-achieving decoder for CQ polar codes. Beyond this question, it remains open as to how BPQM can be generalized to FGs with cycles and also for decoding over general CQ channels. We will investigate these problems in future work.

BPQM also has close connections with the recently introduced notion of *channel* duality [30]. The resulting entropic relations could help characterize the performance of a code over a channel using the performance of its dual code over the dual channel. Since the dual of the pure-state channel is the classical BSC, we believe it may be possible to extend classical techniques for analyzing BP (on BSC), such as density evolution, to analyze BPQM as well.

ACKNOWLEDGMENTS

The authors acknowledge helpful discussions with Prof. Bane Vasic, Prof. Mark Neifeld, Prof. Iman Marvian, Kevin Stubbs, Sarah Brandsen, and Nithin Raveendran. The authors would like to thank Dr. Zachary Dutton for sharing his code to numerically evaluate the YKL limit of decoding a general binary linear code [19]. KPS and SG acknowledge the support of a National Science Foundation (NSF) project "CIF: Medium: Iterative Quantum LDPC Decoders", award number: 1855879, and the Office of Naval Research (ONR) MURI program on Optical Computing, grant number N00014-14-1-0505. The work of NR and HP was supported in part by the National Science Foundation (NSF) under Grant No. 1718494, 1908730 and 1910571. Any opinions, findings, conclusions, and recommendations expressed in this material are those of the authors and do not necessarily reflect the views of these sponsors.

- [1] J. S. Yedidia, W. T. Freeman, and Y. Weiss, Understanding belief propagation and its generalizations, *Exploring artificial intelligence in the new millennium* **8**, 236 (2003).
- [2] J. S. Yedidia, W. T. Freeman, and Y. Weiss, Constructing free energy approximations and generalized belief propagation algorithms, *IEEE Trans. Inform. Theory* **51**, 2282 (2005).
- [3] A. Globerson and T. Jaakkola, Fixing max-product: Convergent message passing algorithms for MAP LP-relaxations, in *Advances in Neural Information Processing Systems 20* (MIT Press, 2007) pp. 553–560.
- [4] Y. Lu, A. Montanari, and B. Prabhakar, Counter braids: Asymptotic optimality of the message passing decoding algorithm, in *Proc. Annual Allerton Conf. on Commun., Control, and Comp.* (2008) pp. 209–216.
- [5] D. L. Donoho, A. Maleki, and A. Montanari, Message passing algorithms for compressed sensing: I. Motivation and construction, in *Proc. IEEE Inform. Theory Workshop* (Cairo, Egypt, 2010).
- [6] M. Bayati and A. Montanari, The dynamics of message passing on dense graphs, with applications to compressed sensing, *IEEE Trans. Inform. Theory* **57**, 764 (2011).
- [7] J. S. Yedidia, Message-passing algorithms for inference and optimization, *Journal of Statistical Physics* **145**, 860 (2011).
- [8] M. Mansour, A message-passing algorithm for graph isomorphism, arXiv preprint arXiv:1704.00395 (2017).
- [9] T. J. Richardson and R. L. Urbanke, *Modern Coding Theory* (Cambridge University Press, New York, NY, 2008).
- [10] S. Kudekar, T. J. Richardson, and R. L. Urbanke, Threshold saturation via spatial coupling: Why convolutional LDPC ensembles perform so well over the BEC, *IEEE Trans. Inform. Theory* **57**, 803 (2011).
- [11] S. Kudekar, T. Richardson, and R. L. Urbanke, Spatially coupled ensembles universally achieve capacity under belief propagation, *IEEE Trans. Inform. Theory* **59**, 7761 (2013).
- [12] S. Kumar, A. J. Young, N. Macris, and H. D. Pfister, Threshold saturation for spatially-coupled LDPC and LDGM codes on BMS channels, *IEEE Trans. Inform. Theory* **60**, 7389 (2014).
- [13] S. Guha and M. M. Wilde, Polar coding to achieve the Holevo capacity of a pure-loss optical channel, in *Proc. IEEE Int. Symp. Inform. Theory* (2012) pp. 546–550.
- [14] C. W. Helstrom, Quantum detection and estimation theory, *Journal of Statistical Physics* **1**, 231 (1969).
- [15] C. W. Helstrom, J. W. Liu, and J. P. Gordon, Quantum-mechanical communication theory, *Proc. of the IEEE* **58**, 1578 (1970).
- [16] S. Dolinar Jr., An Optimum Receiver for the Binary Coherent State Quantum Channel, *MIT Res. Lab. Electron. Q. Prog. Rep.* **111**, 115 (1973).
- [17] E. Arikan, Channel polarization: A method for constructing capacity-achieving codes for symmetric binary-input memoryless channels, *IEEE Trans. Inform. Theory* **55**, 3051 (2009).

- [18] H. Yuen, R. Kennedy, and M. Lax, Optimum testing of multiple hypotheses in quantum detection theory, *IEEE Trans. Inform. Theory* **21**, 125 (1975).
- [19] H. Krovi, S. Guha, Z. Dutton, and M. P. da Silva, Optimal measurements for symmetric quantum states with applications to optical communication, *Phys. Rev. A* **92**, 062333 (2015).
- [20] M. P. Da Silva, S. Guha, and Z. Dutton, Achieving minimum-error discrimination of an arbitrary set of laser-light pulses, *Physical Review A* **87**, 052320 (2013).
- [21] J. M. Renes, Belief propagation decoding of quantum channels by passing quantum messages, *New Journal of Physics* **19**, 072001 (2017).
- [22] M. Hastings, Quantum belief propagation: An algorithm for thermal quantum systems, *Physical Review B* **76**, 201102 (2007).
- [23] M. S. Leifer and D. Poulin, Quantum graphical models and belief propagation, *Annals of Physics* **323**, 1899 (2008).
- [24] M. M. Wilde, *Quantum Information Theory* (Cambridge University Press, 2013).
- [25] T. C. Ralph, A. Gilchrist, G. J. Milburn, W. J. Munro, and S. Glancy, Quantum computation with optical coherent states, *Physical Review A* **68**, 042319 (2003).
- [26] A. Gilchrist, K. Nemoto, W. J. Munro, T. C. Ralph, S. Glancy, S. L. Braunstein, and G. J. Milburn, Schrödinger cats and their power for quantum information processing, *Journal of Optics B: Quantum and Semiclassical Optics* **6**, S828 (2004).
- [27] M. M. Wilde and S. Guha, Polar Codes for Classical-Quantum Channels, *IEEE Trans. Inform. Theory* **59**, 1175 (2013).
- [28] M. A. Nielsen and I. L. Chuang, *Quantum Computation and Quantum Information* (Cambridge University Press, 2010).
- [29] A. Kay, Tutorial on the Quantikz Package, arXiv preprint arXiv:1809.03842 (2018).
- [30] J. M. Renes, Duality of Channels and Codes, *IEEE Trans. Inform. Theory* **64**, 577 (2018).

Appendix A: Circuit Decomposition for Variable Node Unitary and Conditional Rotation

Let $\text{CNOT}_{\theta' \rightarrow \theta} = I_2 \otimes |0\rangle\langle 0| + X \otimes |1\rangle\langle 1|$ be the controlled-NOT operation with the (second) qubit corresponding to angle θ' as the control qubit. Then we observe that

$$\tilde{U}_*(\theta, \theta') := U_*(\theta, \theta') \text{CNOT}_{\theta' \rightarrow \theta} = \begin{bmatrix} a_+ & a_- & 0 & 0 \\ a_- & -a_+ & 0 & 0 \\ 0 & 0 & b_- & b_+ \\ 0 & 0 & -b_+ & b_- \end{bmatrix}, \quad (\text{A1})$$

$$= |0\rangle\langle 0| \otimes \begin{bmatrix} a_+ & a_- \\ a_- & -a_+ \end{bmatrix} + |1\rangle\langle 1| \otimes \begin{bmatrix} b_- & b_+ \\ -b_+ & b_- \end{bmatrix} \quad (\text{A2})$$

$$=: |0\rangle\langle 0| \otimes U_1 + |1\rangle\langle 1| \otimes U_2 \quad (\text{A3})$$

$$= (|0\rangle\langle 0| \otimes U_1 + |1\rangle\langle 1| \otimes I_2) (|0\rangle\langle 0| \otimes I_2 + |1\rangle\langle 1| \otimes U_2). \quad (\text{A4})$$

Let $R_p(\theta) := \exp(-i\frac{\theta}{2}p)$ denote Pauli rotations, where $p \in \{x, y, z\}$ and $i := \sqrt{-1}$. Then the Z - Y decomposition for a single qubit [28, Theorem 4.1] implies that any unitary U can be decomposed as

$$U = e^{i\alpha} R_z(\beta) R_y(\gamma) R_z(\delta) = \begin{bmatrix} e^{i(\alpha-\beta/2-\delta/2)} \cos \frac{\gamma}{2} & -e^{i(\alpha-\beta/2+\delta/2)} \sin \frac{\gamma}{2} \\ e^{i(\alpha+\beta/2-\delta/2)} \sin \frac{\gamma}{2} & e^{i(\alpha+\beta/2+\delta/2)} \cos \frac{\gamma}{2} \end{bmatrix}. \quad (\text{A5})$$

Setting $\gamma_1 := 2\sin^{-1}(a_-)$ and $\gamma_2 := 2\sin^{-1}(b_+)$, we observe that [28, Corollary 4.2]

$$U_1 = \begin{bmatrix} \cos \frac{\gamma_1}{2} & \sin \frac{\gamma_1}{2} \\ \sin \frac{\gamma_1}{2} & -\cos \frac{\gamma_1}{2} \end{bmatrix} = e^{i\frac{\pi}{2}} R_y(\gamma_1) R_z(\pi) =: e^{i\frac{\pi}{2}} A_1 X B_1 X C_1, \quad (\text{A6})$$

$$A_1 := R_y\left(\frac{\gamma_1}{2}\right), \quad (\text{A7})$$

$$B_1 := R_y\left(\frac{-\gamma_1}{2}\right) R_z\left(\frac{-\pi}{2}\right), \quad (\text{A8})$$

$$C_1 := R_z\left(\frac{\pi}{2}\right), \quad (\text{A9})$$

$$U_2 = \begin{bmatrix} \cos \frac{\gamma_2}{2} & \sin \frac{\gamma_2}{2} \\ -\sin \frac{\gamma_2}{2} & \cos \frac{\gamma_2}{2} \end{bmatrix} = e^{i\pi} R_z(\pi) R_y(\gamma_2) R_z(\pi) =: e^{i\pi} A_2 X B_2 X, \quad (\text{A10})$$

$$A_2 := R_z(\pi) R_y(\gamma_2/2), \quad (\text{A11})$$

$$B_2 := R_y(-\gamma_2/2) R_z(-\pi). \quad (\text{A12})$$

Then we can express the full circuit decomposition for $U_*(\theta, \theta')$ as shown in Fig. 11.

Similarly, the rotations K_+ and K_- defined in (55) can be expressed as

$$K_+ = \frac{1}{\sqrt{2}} \begin{bmatrix} \cos \frac{\varphi_{00}^*}{2} + \sin \frac{\varphi_{00}^*}{2} & \cos \frac{\varphi_{00}^*}{2} - \sin \frac{\varphi_{00}^*}{2} \\ \sin \frac{\varphi_{00}^*}{2} - \cos \frac{\varphi_{00}^*}{2} & \sin \frac{\varphi_{00}^*}{2} + \cos \frac{\varphi_{00}^*}{2} \end{bmatrix} \quad (\text{A13})$$

$$=: \begin{bmatrix} \cos \frac{\gamma}{2} & \sin \frac{\gamma}{2} \\ -\sin \frac{\gamma}{2} & \cos \frac{\gamma}{2} \end{bmatrix} \quad (\text{A14})$$

$$= e^{i\pi} R_z(\pi) R_y(\gamma) R_z(\pi) \quad (\text{A15})$$

$$=: e^{i\pi} A_+ X B_+ X, \quad (\text{A16})$$

$$K_- = \frac{1}{\sqrt{2}} \begin{bmatrix} \sin \frac{\varphi_{00}^*}{2} + \cos \frac{\varphi_{00}^*}{2} & \sin \frac{\varphi_{00}^*}{2} - \cos \frac{\varphi_{00}^*}{2} \\ \cos \frac{\varphi_{00}^*}{2} - \sin \frac{\varphi_{00}^*}{2} & \cos \frac{\varphi_{00}^*}{2} + \sin \frac{\varphi_{00}^*}{2} \end{bmatrix} \quad (\text{A17})$$

$$= K_+^\dagger, \quad (\text{A18})$$

$$\text{where } \gamma := 2 \sin^{-1} \left[\frac{1}{\sqrt{2}} \left(\cos \frac{\varphi_{00}^*}{2} - \sin \frac{\varphi_{00}^*}{2} \right) \right], \quad (\text{A19})$$

$$A_+ := R_z(\pi) R_y \left(\frac{\gamma}{2} \right), \quad (\text{A20})$$

$$B_+ := R_y \left(\frac{-\gamma}{2} \right) R_z(-\pi). \quad (\text{A21})$$

The coherently controlled gate M_{m_1} defined in (55) is decomposed in Fig. 12 using the above calculations.

Appendix B: Calculations for Node Convolutions

The variable and check node convolutions are given by

$$[W \circledast W'](x) = W(x) \otimes W'(x), \quad (\text{B1})$$

$$[W \boxtimes W'](x) = \frac{1}{2}(W(x) \otimes W'(0) + W(x+1) \otimes W'(1)). \quad (\text{B2})$$

The channel outputs for a pure state channel are $|\pm\theta\rangle$, where

$$|\pm\theta\rangle = \cos \frac{\theta}{2} |0\rangle \pm \sin \frac{\theta}{2} |1\rangle. \quad (\text{B3})$$

The overlap between the two outputs is given by $\langle -\theta | \theta \rangle = \cos^2 \frac{\theta}{2} - \sin^2 \frac{\theta}{2} = \cos \theta$. The Helstrom measurement projects onto $|\pm\frac{\pi}{2}\rangle$.

The Stinespring's representation for a classical-quantum (CQ) channel W that maps density states from Hilbert space \mathcal{H}_A to \mathcal{H}_B is given by

$$W(x) := \text{Tr}_E \left[V_{BE|A} |x\rangle \langle x| V_{BE|A}^\dagger \right], \quad (\text{B4})$$

where \mathcal{H}_E is an ancilla space and $V_{BE|A}$ is an isometry that maps \mathcal{H}_A to $\mathcal{H}_B \otimes \mathcal{H}_E$. Therefore, even for a pure state channel W , we must take its outputs to be density states $|\pm\theta\rangle \langle \pm\theta|$ and not $|\pm\theta\rangle$. On the contrary, if we take it to be $|\pm\theta\rangle$ then we immediately notice that the output state of the check convolution in (B2) above is not normalized and hence does not represent a physical operation.

1. Variable Node Convolution

The convolution $W \circledast W'$ outputs (the density state for) either $|\theta^*\rangle := |\theta\rangle \otimes |\theta'\rangle$ or $|- \theta^*\rangle := |-\theta\rangle \otimes |-\theta'\rangle$, which are again two pure states with an overlap angle θ^* given by

$$\cos \theta^* := \langle -\theta^* | \theta^* \rangle = (\langle -\theta | \otimes \langle -\theta' |) \cdot (|\theta\rangle \otimes |\theta'\rangle) = \langle -\theta | \theta \rangle \otimes \langle -\theta' | \theta' \rangle = \cos \theta \cos \theta'. \quad (\text{B5})$$

The following unitary transformation compresses the states to the first qubit, leaving the second in the state $|0\rangle$:

$$U_{\otimes}(\theta, \theta') := \begin{bmatrix} a_+ & 0 & 0 & a_- \\ a_- & 0 & 0 & -a_+ \\ 0 & b_+ & b_- & 0 \\ 0 & b_- & -b_+ & 0 \end{bmatrix}, \quad (\text{B6})$$

where

$$a_{\pm} = \frac{1}{\sqrt{2}} \frac{\cos\left(\frac{\theta-\theta'}{2}\right) \pm \cos\left(\frac{\theta+\theta'}{2}\right)}{\sqrt{1+\cos\theta\cos\theta'}}, \quad b_{\pm} = \frac{1}{\sqrt{2}} \frac{\sin\left(\frac{\theta+\theta'}{2}\right) \mp \sin\left(\frac{\theta-\theta'}{2}\right)}{\sqrt{1-\cos\theta\cos\theta'}}. \quad (\text{B7})$$

Let us verify by explicit calculation that

$$U_{\otimes}(\theta, \theta') (|\pm\theta\rangle\langle\pm\theta| \otimes |\pm\theta'\rangle\langle\pm\theta'|) U_{\otimes}^{\dagger}(\theta, \theta') = |\pm\theta^{\otimes}\rangle\langle\pm\theta^{\otimes}| \otimes |0\rangle\langle 0|, \quad (\text{B8})$$

where $|\pm\theta^{\otimes}\rangle := \sqrt{p_0}|0\rangle \pm \sqrt{p_1}|1\rangle$, $p_0 := \frac{1}{2}(1 + \cos\theta\cos\theta')$, $p_1 := 1 - p_0 = \frac{1}{2}(1 - \cos\theta\cos\theta')$.

$$|\pm\theta^{\otimes}\rangle := \begin{bmatrix} \sqrt{\frac{1+\cos\theta\cos\theta'}{2}} \\ \pm\sqrt{\frac{1-\cos\theta\cos\theta'}{2}} \end{bmatrix} = \begin{bmatrix} \sqrt{\frac{1+\cos\theta^{\otimes}}{2}} \\ \pm\sqrt{\frac{1-\cos\theta^{\otimes}}{2}} \end{bmatrix} = \begin{bmatrix} \cos\frac{\theta^{\otimes}}{2} \\ \pm\sin\frac{\theta^{\otimes}}{2} \end{bmatrix} = \cos\frac{\theta^{\otimes}}{2}|0\rangle \pm \sin\frac{\theta^{\otimes}}{2}|1\rangle. \quad (\text{B9})$$

First, using the definitions for $|\pm\theta\rangle$ and $|\pm\theta'\rangle$ we have

$$|\pm\theta\rangle\otimes|\pm\theta'\rangle = \cos\frac{\theta}{2}\cos\frac{\theta'}{2}|00\rangle \pm \cos\frac{\theta}{2}\sin\frac{\theta'}{2}|01\rangle \pm \sin\frac{\theta}{2}\cos\frac{\theta'}{2}|10\rangle + \sin\frac{\theta}{2}\sin\frac{\theta'}{2}|11\rangle \quad (\text{B10})$$

$$= \left[\cos\frac{\theta}{2}\cos\frac{\theta'}{2}, \pm\cos\frac{\theta}{2}\sin\frac{\theta'}{2}, \pm\sin\frac{\theta}{2}\cos\frac{\theta'}{2}, \sin\frac{\theta}{2}\sin\frac{\theta'}{2} \right]^T. \quad (\text{B11})$$

Hence we get

$$|\pm\psi\rangle := U_{\otimes}(\theta, \theta') (|\pm\theta\rangle\otimes|\pm\theta'\rangle) = \begin{bmatrix} a_+ \cos\frac{\theta}{2}\cos\frac{\theta'}{2} + a_- \sin\frac{\theta}{2}\sin\frac{\theta'}{2} \\ a_- \cos\frac{\theta}{2}\cos\frac{\theta'}{2} - a_+ \sin\frac{\theta}{2}\sin\frac{\theta'}{2} \\ \pm b_+ \cos\frac{\theta}{2}\sin\frac{\theta'}{2} \pm b_- \sin\frac{\theta}{2}\cos\frac{\theta'}{2} \\ \pm b_- \cos\frac{\theta}{2}\sin\frac{\theta'}{2} \mp b_+ \sin\frac{\theta}{2}\cos\frac{\theta'}{2} \end{bmatrix} =: \begin{bmatrix} \psi_{00} \\ \psi_{01} \\ \psi_{10} \\ \psi_{11} \end{bmatrix}. \quad (\text{B12})$$

For convenience let us make some definitions:

$$\alpha := \cos\frac{\theta-\theta'}{2} + \cos\frac{\theta+\theta'}{2} = \frac{1}{2}\cos\frac{\theta}{2}\cos\frac{\theta'}{2}, \quad \beta := \cos\frac{\theta-\theta'}{2} - \cos\frac{\theta+\theta'}{2} = \frac{1}{2}\sin\frac{\theta}{2}\sin\frac{\theta'}{2}, \quad (\text{B13})$$

$$\gamma := \sin\frac{\theta+\theta'}{2} - \sin\frac{\theta-\theta'}{2} = \frac{1}{2}\cos\frac{\theta}{2}\sin\frac{\theta'}{2}, \quad \delta := \sin\frac{\theta+\theta'}{2} + \sin\frac{\theta-\theta'}{2} = \frac{1}{2}\sin\frac{\theta}{2}\cos\frac{\theta'}{2}. \quad (\text{B14})$$

Then using the identities $\cos\theta = 2\cos^2\frac{\theta}{2} - 1 = 1 - 2\sin^2\frac{\theta}{2}$ we see that

$$\psi_{00} = \frac{1}{2} [a_+\alpha + a_-\beta] = \frac{1}{2\sqrt{2}} \frac{2 \left[\cos^2\frac{\theta-\theta'}{2} + \cos^2\frac{\theta+\theta'}{2} \right]}{\sqrt{1+\cos\theta\cos\theta'}} = \sqrt{\frac{1+\cos\theta\cos\theta'}{2}}, \quad (\text{B15})$$

$$\psi_{01} = \frac{1}{2} [a_-\alpha - a_+\beta] = \frac{1}{2\sqrt{2}} \frac{\alpha\beta - \beta\alpha}{\sqrt{1+\cos\theta\cos\theta'}} = 0, \quad (\text{B16})$$

$$\psi_{10} = \frac{1}{2} [\pm b_+\gamma \pm b_-\delta] = \frac{1}{2\sqrt{2}} \frac{2 \left[\pm\sin^2\frac{\theta+\theta'}{2} \pm \sin^2\frac{\theta-\theta'}{2} \right]}{\sqrt{1-\cos\theta\cos\theta'}} = \pm\sqrt{\frac{1-\cos\theta\cos\theta'}{2}}, \quad (\text{B17})$$

$$\psi_{11} = \frac{1}{2} [\pm b_-\gamma \mp b_+\delta] = \frac{1}{2\sqrt{2}} \frac{\pm\gamma\delta \mp \delta\gamma}{\sqrt{1-\cos\theta\cos\theta'}} = 0. \quad (\text{B18})$$

Therefore we find that $|\pm\psi\rangle = |\pm\theta^{\otimes}\rangle\otimes|0\rangle$ and hence

$$U_{\otimes}(\theta, \theta') (|\pm\theta\rangle\langle\pm\theta| \otimes |\pm\theta'\rangle\langle\pm\theta'|) U_{\otimes}^{\dagger}(\theta, \theta') = |\pm\psi\rangle\langle\pm\psi| = |\pm\theta^{\otimes}\rangle\langle\pm\theta^{\otimes}| \otimes |0\rangle\langle 0|. \quad (\text{B19})$$

2. Factor Node Convolution

The result of $W \boxtimes W$ is not pure and hence we would like to unitarily transform the output of the \boxtimes convolution to a CQ state of the form

$$\Psi_{\text{desired}} := \sum_{j \in \{0,1\}} p_j |\pm\theta_j^{\boxtimes}\rangle \langle \pm\theta_j^{\boxtimes}| \otimes |j\rangle \langle j|, \quad (\text{B20})$$

for some appropriate state $|\pm\theta_j^{\boxtimes}\rangle$ and probabilities p_j . It turns out that the unitary operation $U_{\boxtimes} := \text{CNOT}_{1 \rightarrow 2}$ is the correct one. Let us verify that by explicit calculation for inputs $x = 0$ and $x = 1$ simultaneously. We have

$$[W \boxtimes W'](x) = \frac{1}{2} (W(x) \otimes W'(0) + W(x \oplus 1) \otimes W'(1)) \quad (\text{B21})$$

$$= \frac{1}{2} \left(|\pm\theta\rangle \langle \pm\theta| \otimes |\theta'\rangle \langle \theta'| + |\mp\theta\rangle \langle \mp\theta| \otimes |-\theta'\rangle \langle -\theta'| \right) \quad (\pm \equiv (-1)^x, \mp \equiv (-1)^{x \oplus 1}) \quad (\text{B22})$$

$$:= \frac{1}{2} (\tilde{\varphi}_1 + \tilde{\varphi}_2). \quad (\text{B23})$$

$$\Rightarrow \Psi := U_{\boxtimes} \left([W \boxtimes W'](x) \right) U_{\boxtimes}^{\dagger} \quad (\text{B24})$$

$$= \frac{1}{2} (U_{\boxtimes} \tilde{\varphi}_1 U_{\boxtimes}^{\dagger} + U_{\boxtimes} \tilde{\varphi}_2 U_{\boxtimes}^{\dagger}) \quad (\text{B25})$$

$$:= \frac{1}{2} (\varphi_1 + \varphi_2). \quad (\text{B26})$$

Now we calculate φ_1 and φ_2 separately. We first have

$$\begin{aligned} \tilde{\varphi}_1 &= |\pm\theta\rangle \langle \pm\theta| \otimes |\theta'\rangle \langle \theta'| \\ &= (|\pm\theta\rangle \otimes |\theta'\rangle) \cdot (|\pm\theta\rangle \otimes \langle \theta'|) \end{aligned} \quad (\text{B27})$$

$$\begin{aligned} &= \left[\cos \frac{\theta}{2} \cos \frac{\theta'}{2} |0\rangle \langle 0| + \cos \frac{\theta}{2} \sin \frac{\theta'}{2} |0\rangle \langle 1| \pm \sin \frac{\theta}{2} \cos \frac{\theta'}{2} |1\rangle \langle 0| \pm \sin \frac{\theta}{2} \sin \frac{\theta'}{2} |1\rangle \langle 1| \right] \\ &\otimes \left[\cos \frac{\theta}{2} \cos \frac{\theta'}{2} \langle 0| \langle 0| + \cos \frac{\theta}{2} \sin \frac{\theta'}{2} \langle 0| \langle 1| \pm \sin \frac{\theta}{2} \cos \frac{\theta'}{2} \langle 1| \langle 0| \pm \sin \frac{\theta}{2} \sin \frac{\theta'}{2} \langle 1| \langle 1| \right] \end{aligned} \quad (\text{B28})$$

$$\begin{aligned} \Rightarrow \varphi_1 &= \text{CNOT}_{1 \rightarrow 2} (\tilde{\varphi}_1) \text{CNOT}_{1 \rightarrow 2} \\ &= \left[\cos \frac{\theta}{2} \cos \frac{\theta'}{2} |0\rangle \langle 0| + \cos \frac{\theta}{2} \sin \frac{\theta'}{2} |0\rangle \langle 1| \pm \sin \frac{\theta}{2} \sin \frac{\theta'}{2} |1\rangle \langle 0| \pm \sin \frac{\theta}{2} \cos \frac{\theta'}{2} |1\rangle \langle 1| \right] \\ &\otimes \left[\cos \frac{\theta}{2} \cos \frac{\theta'}{2} \langle 0| \langle 0| + \cos \frac{\theta}{2} \sin \frac{\theta'}{2} \langle 0| \langle 1| \pm \sin \frac{\theta}{2} \sin \frac{\theta'}{2} \langle 1| \langle 0| \pm \sin \frac{\theta}{2} \cos \frac{\theta'}{2} \langle 1| \langle 1| \right] \end{aligned} \quad (\text{B29})$$

$$\begin{aligned} &= \left[\cos^2 \frac{\theta}{2} \cos^2 \frac{\theta'}{2} |0\rangle \langle 0| \pm \frac{1}{4} \sin \theta \sin \theta' (|0\rangle \langle 1| + |1\rangle \langle 0|) + \sin^2 \frac{\theta}{2} \sin^2 \frac{\theta'}{2} |1\rangle \langle 1| \right] \otimes |0\rangle \langle 0| \\ &+ \left[\cos^2 \frac{\theta}{2} \sin^2 \frac{\theta'}{2} |0\rangle \langle 0| \pm \frac{1}{4} \sin \theta \sin \theta' (|0\rangle \langle 1| + |1\rangle \langle 0|) + \sin^2 \frac{\theta}{2} \cos^2 \frac{\theta'}{2} |1\rangle \langle 1| \right] \otimes |1\rangle \langle 1| \\ &+ \frac{1}{2} \left[\cos^2 \frac{\theta}{2} \sin \theta' |0\rangle \langle 0| \pm \sin \theta \cos^2 \frac{\theta'}{2} |0\rangle \langle 1| \pm \sin \theta \sin^2 \frac{\theta'}{2} |1\rangle \langle 0| + \sin^2 \frac{\theta}{2} \sin \theta' |1\rangle \langle 1| \right] \otimes |0\rangle \langle 1| \\ &+ \frac{1}{2} \left[\cos^2 \frac{\theta}{2} \sin \theta' |0\rangle \langle 0| \pm \sin \theta \sin^2 \frac{\theta'}{2} |0\rangle \langle 1| \pm \sin \theta \cos^2 \frac{\theta'}{2} |1\rangle \langle 0| + \sin^2 \frac{\theta}{2} \sin \theta' |1\rangle \langle 1| \right] \otimes |1\rangle \langle 0|. \end{aligned} \quad (\text{B30})$$

Similarly we get

$$\begin{aligned} \tilde{\varphi}_2 &= |\mp\theta\rangle \langle \mp\theta| \otimes |-\theta'\rangle \langle -\theta'| \\ &= (|\mp\theta\rangle \otimes |-\theta'\rangle) \cdot (|\mp\theta\rangle \otimes \langle -\theta'|) \end{aligned} \quad (\text{B31})$$

$$\begin{aligned} &= \left[\cos \frac{\theta}{2} \cos \frac{\theta'}{2} |0\rangle \langle 0| - \cos \frac{\theta}{2} \sin \frac{\theta'}{2} |0\rangle \langle 1| \mp \sin \frac{\theta}{2} \cos \frac{\theta'}{2} |1\rangle \langle 0| \pm \sin \frac{\theta}{2} \sin \frac{\theta'}{2} |1\rangle \langle 1| \right] \\ &\otimes \left[\cos \frac{\theta}{2} \cos \frac{\theta'}{2} \langle 0| \langle 0| - \cos \frac{\theta}{2} \sin \frac{\theta'}{2} \langle 0| \langle 1| \mp \sin \frac{\theta}{2} \cos \frac{\theta'}{2} \langle 1| \langle 0| \pm \sin \frac{\theta}{2} \sin \frac{\theta'}{2} \langle 1| \langle 1| \right] \end{aligned} \quad (\text{B32})$$

$$\begin{aligned}
\Rightarrow \varphi_2 &= \text{CNOT}_{1 \rightarrow 2} (\tilde{\varphi}_2) \text{CNOT}_{1 \rightarrow 2} \\
&= \left[\cos \frac{\theta}{2} \cos \frac{\theta'}{2} |0\rangle \langle 0\rangle - \cos \frac{\theta}{2} \sin \frac{\theta'}{2} |0\rangle \langle 1\rangle \pm \sin \frac{\theta}{2} \sin \frac{\theta'}{2} |1\rangle \langle 0\rangle \mp \sin \frac{\theta}{2} \cos \frac{\theta'}{2} |1\rangle \langle 1\rangle \right] \\
&\otimes \left[\cos \frac{\theta}{2} \cos \frac{\theta'}{2} \langle 0| \langle 0| - \cos \frac{\theta}{2} \sin \frac{\theta'}{2} \langle 0| \langle 1| \pm \sin \frac{\theta}{2} \sin \frac{\theta'}{2} \langle 1| \langle 0| \mp \sin \frac{\theta}{2} \cos \frac{\theta'}{2} \langle 1| \langle 1| \right] \tag{B33}
\end{aligned}$$

$$\begin{aligned}
&= \left[\cos^2 \frac{\theta}{2} \cos^2 \frac{\theta'}{2} |0\rangle \langle 0| \pm \frac{1}{4} \sin \theta \sin \theta' (|0\rangle \langle 1| + |1\rangle \langle 0|) + \sin^2 \frac{\theta}{2} \sin^2 \frac{\theta'}{2} |1\rangle \langle 1| \right] \otimes |0\rangle \langle 0| \\
&+ \left[\cos^2 \frac{\theta}{2} \sin^2 \frac{\theta'}{2} |0\rangle \langle 0| \pm \frac{1}{4} \sin \theta \sin \theta' (|0\rangle \langle 1| + |1\rangle \langle 0|) + \sin^2 \frac{\theta}{2} \cos^2 \frac{\theta'}{2} |1\rangle \langle 1| \right] \otimes |1\rangle \langle 1| \\
&+ \frac{1}{2} \left[-\cos^2 \frac{\theta}{2} \sin \theta' |0\rangle \langle 0| \mp \sin \theta \cos^2 \frac{\theta'}{2} |0\rangle \langle 1| \mp \sin \theta \sin^2 \frac{\theta'}{2} |1\rangle \langle 0| - \sin^2 \frac{\theta}{2} \sin \theta' |1\rangle \langle 1| \right] \otimes |0\rangle \langle 1| \\
&+ \frac{1}{2} \left[-\cos^2 \frac{\theta}{2} \sin \theta' |0\rangle \langle 0| \mp \sin \theta \sin^2 \frac{\theta'}{2} |0\rangle \langle 1| \mp \sin \theta \cos^2 \frac{\theta'}{2} |1\rangle \langle 0| - \sin^2 \frac{\theta}{2} \sin \theta' |1\rangle \langle 1| \right] \otimes |1\rangle \langle 0|. \tag{B34}
\end{aligned}$$

Therefore we get

$$\begin{aligned}
\Psi &= \frac{1}{2} (\varphi_1 + \varphi_2) \\
&= \left[\cos^2 \frac{\theta}{2} \cos^2 \frac{\theta'}{2} |0\rangle \langle 0| \pm \frac{1}{4} \sin \theta \sin \theta' (|0\rangle \langle 1| + |1\rangle \langle 0|) + \sin^2 \frac{\theta}{2} \sin^2 \frac{\theta'}{2} |1\rangle \langle 1| \right] \otimes |0\rangle \langle 0| \\
&+ \left[\cos^2 \frac{\theta}{2} \sin^2 \frac{\theta'}{2} |0\rangle \langle 0| \pm \frac{1}{4} \sin \theta \sin \theta' (|0\rangle \langle 1| + |1\rangle \langle 0|) + \sin^2 \frac{\theta}{2} \cos^2 \frac{\theta'}{2} |1\rangle \langle 1| \right] \otimes |1\rangle \langle 1| \tag{B35}
\end{aligned}$$

$$\begin{aligned}
&= \frac{1}{4} \left[(1 + \cos \theta)(1 + \cos \theta') |0\rangle \langle 0| \pm \sin \theta \sin \theta' (|0\rangle \langle 1| + |1\rangle \langle 0|) + (1 - \cos \theta)(1 - \cos \theta') |1\rangle \langle 1| \right] \otimes |0\rangle \langle 0| \\
&+ \frac{1}{4} \left[(1 + \cos \theta)(1 - \cos \theta') |0\rangle \langle 0| \pm \sin \theta \sin \theta' (|0\rangle \langle 1| + |1\rangle \langle 0|) + (1 - \cos \theta)(1 + \cos \theta') |1\rangle \langle 1| \right] \otimes |1\rangle \langle 1|. \tag{B36}
\end{aligned}$$

Now let us define two new angles $\theta_0^{\boxtimes}, \theta_1^{\boxtimes}$ as

$$\cos \theta_0^{\boxtimes} := \frac{\cos \theta + \cos \theta'}{1 + \cos \theta \cos \theta'}, \quad \cos \theta_1^{\boxtimes} := \frac{\cos \theta - \cos \theta'}{1 - \cos \theta \cos \theta'}. \tag{B37}$$

Note that these are the two possible overlaps after applying the check node unitary operation.

This gives us the following identities:

$$\begin{aligned}
\cos \frac{\theta_0^{\boxtimes}}{2} &= \sqrt{\frac{1}{2} (1 + \cos \theta_0^{\boxtimes})} = \sqrt{\frac{1}{2} \frac{(1 + \cos \theta)(1 + \cos \theta')}{1 + \cos \theta \cos \theta'}}; \quad \cos \frac{\theta_1^{\boxtimes}}{2} = \sqrt{\frac{1}{2} \frac{(1 + \cos \theta)(1 - \cos \theta')}{1 - \cos \theta \cos \theta'}} \\
\sin \frac{\theta_0^{\boxtimes}}{2} &= \sqrt{\frac{1}{2} (1 - \cos \theta_0^{\boxtimes})} = \sqrt{\frac{1}{2} \frac{(1 - \cos \theta)(1 - \cos \theta')}{1 + \cos \theta \cos \theta'}}; \quad \sin \frac{\theta_1^{\boxtimes}}{2} = \sqrt{\frac{1}{2} \frac{(1 - \cos \theta)(1 + \cos \theta')}{1 - \cos \theta \cos \theta'}} \\
\cos \frac{\theta_0^{\boxtimes}}{2} \sin \frac{\theta_0^{\boxtimes}}{2} &= \frac{1}{2} \frac{\sin \theta \sin \theta'}{(1 + \cos \theta \cos \theta')}; \quad \cos \frac{\theta_1^{\boxtimes}}{2} \sin \frac{\theta_1^{\boxtimes}}{2} = \frac{1}{2} \frac{\sin \theta \sin \theta'}{(1 - \cos \theta \cos \theta')} \tag{B38}
\end{aligned}$$

Using these new angles and their identities in (B36) we get

$$\begin{aligned}
\Psi &= \frac{1}{2} (1 + \cos \theta \cos \theta') \left[\cos^2 \frac{\theta_0^{\boxtimes}}{2} |0\rangle \langle 0| \pm \cos \frac{\theta_0^{\boxtimes}}{2} \sin \frac{\theta_0^{\boxtimes}}{2} (|0\rangle \langle 1| + |1\rangle \langle 0|) + \sin^2 \frac{\theta_0^{\boxtimes}}{2} |1\rangle \langle 1| \right] \otimes |0\rangle \langle 0| \\
&+ \frac{1}{2} (1 - \cos \theta \cos \theta') \left[\cos^2 \frac{\theta_1^{\boxtimes}}{2} |0\rangle \langle 0| \pm \cos \frac{\theta_1^{\boxtimes}}{2} \sin \frac{\theta_1^{\boxtimes}}{2} (|0\rangle \langle 1| + |1\rangle \langle 0|) + \sin^2 \frac{\theta_1^{\boxtimes}}{2} |1\rangle \langle 1| \right] \otimes |1\rangle \langle 1| \tag{B39}
\end{aligned}$$

$$= p_0 |\pm \theta_0^{\boxtimes}\rangle \langle \pm \theta_0^{\boxtimes}| \otimes |0\rangle \langle 0| + p_1 |\pm \theta_1^{\boxtimes}\rangle \langle \pm \theta_1^{\boxtimes}| \otimes |1\rangle \langle 1| \tag{B40}$$

$$\Rightarrow \Psi = \sum_{j \in \{0,1\}} p_j |\pm \theta_j^{\boxtimes}\rangle \langle \pm \theta_j^{\boxtimes}| \otimes |j\rangle \langle j|, \tag{B41}$$

where $p_0 := \frac{1}{2} (1 + \cos \theta \cos \theta')$, $p_1 := 1 - p_0 = \frac{1}{2} (1 - \cos \theta \cos \theta')$ and $|\pm \theta_j^{\boxtimes}\rangle := \cos \frac{\theta_j^{\boxtimes}}{2} |0\rangle \pm \sin \frac{\theta_j^{\boxtimes}}{2} |1\rangle$ for $j = 0, 1$. This is what we desired to get initially in (B20).